NEUROPHYSIOLOGY

Fear extinction relies on ventral hippocampal safety codes shaped by the amygdala

Robin Nguyen*†, Konstantinos Koukoutselos, Thomas Forro, Stéphane Ciocchi*

Extinction memory retrieval is influenced by spatial contextual information that determines responding to conditioned stimuli (CS). However, it is poorly understood whether contextual representations are imbued with emotional values to support memory selection. Here, we performed activity-dependent engram tagging and in vivo single-unit electrophysiological recordings from the ventral hippocampus (vH) while optogenetically manipulating basolateral amygdala (BLA) inputs during the formation of cued fear extinction memory. During fear extinction when CS acquire safety properties, we found that CS-related activity in the vH reactivated during sleep consolidation and was strengthened upon memory retrieval. Moreover, fear extinction memory was facilitated when the extinction context exhibited precise coding of its affective zones. Last, these activity patterns along with the retrieval of the fear extinction memory were dependent on glutamatergic transmission from the BLA during extinction learning. Thus, fear extinction memory relies on the formation of contextual and stimulus safety representations in the vH instructed by the BLA.

INTRODUCTION

Memory of environments where salient events have occurred is essential for guiding adaptive behavior. When a stimulus is associated with multiple outcomes, context acts as an occasion setter disambiguating the stimulus's meaning (*1*–*3*). Defensive reactions to a threat-associated stimulus can be suppressed upon learning that the stimulus no longer predicts threat—a process termed fear extinction—in which the conditioned stimuli (CS) is repeatedly encountered in the absence of the aversive unconditioned stimulus (US). This contingency (i.e., CS—no-US association) leads to the formation of a new safety memory reflecting that the threat will not occur (*2*, *4*, *5*). Unlike the original fear memory, the opposing extinction memory is context dependent, being selectively retrieved in the spatial environment where learning took place. Encountering the CS in the original fear context or in a neutral context following extinction learning elicits fear memory retrieval (i.e., CS—US association) (*6*).

A core brain structure serving both fear and extinction learning is the amygdala (*7*–*9*). Fear extinction learning involves the coordinated activity of neuronal populations in the amygdala to inhibit midbrain-mediated fear expression (*10*–*13*). Segregated populations of basolateral amygdala (BLA) neurons respond to the same CS during expression of either fear or extinction memories (*10*, *14*). Concomitantly, large-scale cortical and subcortical circuit interactions mediate state-dependent regulation of fear and extinction memory retrieval (*15*–*19*).

The influence of context on fear memory retrieval may arise via the reciprocal monosynaptic connections between the ventral hippocampus (vH) and the BLA (*20*, *21*). Contextual representations in the vH are thought to be transmitted to downstream regions involved in the processing of CS, their associated values, and behavioral outcomes (*3*), such as the medial prefrontal cortex, nucleus accumbens, and BLA (*22*). The vH has been demonstrated to play a crucial role in the encoding and retrieval of emotionally salient contextual memories (*23*–*26*). Distinct neuronal populations in the vH are selectively active in contexts associated with threatening or rewarding stimuli (*24*, *26*–*31*). Moreover, in maze assays of anxiety, vH neurons exhibit spatial activity patterns that map onto affective zones, including preferential firing in the open or closed arms of elevated plus mazes (*24*, *25*, *28*, *29*), and in the center of large open arenas (*28*). However, the spatial mapping of contexts with acquired valence by vH neurons is less well understood. Furthermore, studies examining the contribution of the vH to context-dependent fear memory have mostly investigated its role in facilitating contextual fear memory or fear renewal (*27*–*30*, *32*–*34*), although evidence exists for its involvement in extinction learning (*35*, *36*). BLA projections to the vH have been found to modulate affective states (*37*, *38*) and signal the valence of CS (*39*), pointing to the potential involvement of this circuit in fear extinction.

Using in vivo electrophysiological recordings from the vH with optogenetic inhibition of BLA monosynaptic inputs and activity-dependent engram tagging, we demonstrate that activity in the BLA-vH circuit is essential for the formation of fear extinction memory and for the emergence of vH neuronal representations of the extinction CS and context. These findings reveal that the BLA instructs the formation of neuronal representations of contextual and stimulus safety in the vH to support fear extinction memory.

RESULTS

BLA projections to the vH are required for extinction memory formation

The vH receives multimodal information that may imbed sensory properties, contingencies, and valence into contextual representations during learning. To determine which brain regions could serve as major monosynaptic input sources to vH neurons subserving an extinction memory engram, we performed trans-synaptic

Laboratory of Systems Neuroscience, Department of Physiology, University of Bern, Bern, Switzerland.
*Corresponding author. Email: stephane.ciocchi@unibe.ch (S.C.); rn2560@columbia.edu (R.N.)
†Present address: Department of Neuroscience, The Kavli Institute for Brain Science, Mortimer B. Zuckerman Mind Brain Behavior Institute, Jerome L. Greene Science Center, Columbia University, New York, NY, USA.

retrograde tracing from vH neurons activated in the context in which fear extinction took place. This strategy was accomplished by using Fos-TRAP2 mice in combination with the pseudotyped glycoprotein (G)–deleted rabies approach (*40*, *41*). Fos$^{2A\text{-}iCreERT2}$ (TRAP2) mice were first infused with Cre-dependent adeno-associated virus (AAV) containing the avian tumor virus A receptor (TVA) and G (AAV9-hsyn-DIO-TVA-2A-EGFP-2A-oG) in the vH and after 2 weeks underwent discriminative auditory fear conditioning and extinction training in distinct contexts (Fig. 1A). On the extinction memory test day, mice were either exposed to the extinction context (Ext-TRAPed) or remained in the home cage as a control and immediately after received an intraperitoneal injection of 4-hydroxytamoxifen [4-OHT; 50 mg/kg intraperitoneal (ip)]. After 1 week, we delivered envelope-A–pseudotyped G-deleted rabies (EnvA-RVdG-tdTomato) to the vH. Neurons active in close temporal proximity to the 4-OHT

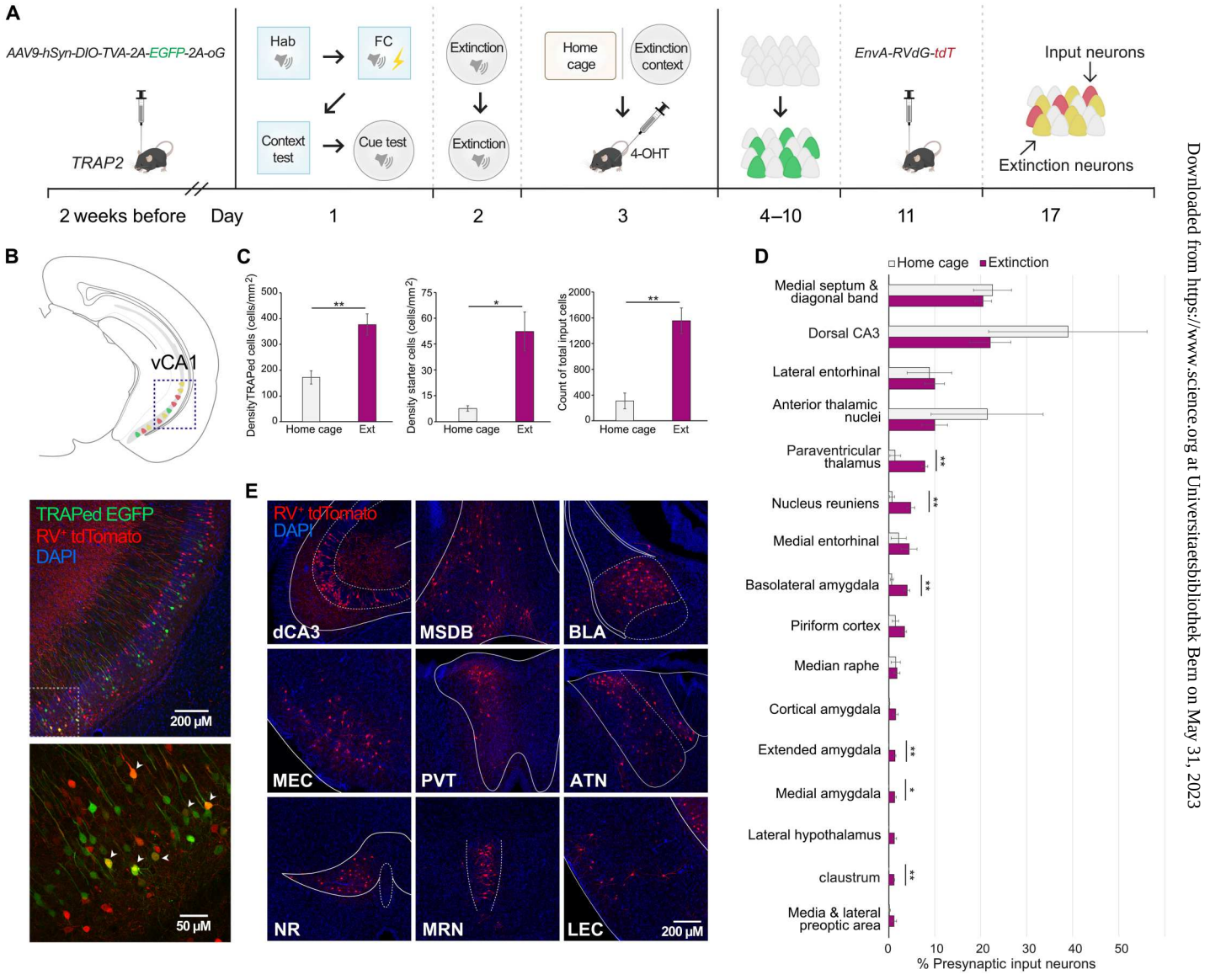

Fig. 1. Brain-wide inputs to vH fear extinction tagged neurons. (**A**) Experimental protocol for rabies tracing from ventral hippocampus (vH) extinction-context memory neurons. 4-OHT, 4-hydroxytamoxifen. FC, fear conditioning. (**B**) Top, schematic; middle, representative expression in vH. Enhanced green fluorescent protein (EGFP) in Ext-TRAPed neurons and tdTomato in RV-infected neurons. RV, rabies virus. Bottom: Magnified view of middle boxed area, arrowheads point to Ext-TRAPed/RV$^+$ double-labeled starter neurons. DAPI, 4′,6-diamidino-2-phenylindole. (**C**) Left: Density of vH Fos-TRAPed neurons. Home cage (HC) versus extinction (Ext): $t_{(7)} = 3.93$, $P = 0.0057$. Middle: Density of double-labeled starter neurons. HC versus Ext: $t_{(7)} = 3.47$, $P = 0.0104$. Right: Density of tdTomato-labeled input neurons. HC versus Ext: $t_{(7)} = 4.94$, $P = 0.0017$. Unpaired *t* tests. (**D**) Whole-brain quantification of percent RV$^+$ tdTomato neurons out of total tdTomato neurons. Regions sorted in descending order by percentage, and only regions >1% are shown. Paraventricular thalamus: $P = 0.0055$, nucleus reuniens: $P = 0.0061$, basal amygdala (BLA): $P = 0.0032$, medial amygdala: $P = 0.0136$, extended amygdala: $P = 0.0033$, and claustrum: $P = 0.0013$. Unpaired *t* tests corrected with two-stage step-up method of Benjamini, Krieger, and Yekutieli [false discovery rate (FDR) = 0.05]. (**E**) Representative expression of RV$^+$ tdTomato-labeled neurons in major presynaptic input regions to vH Ext-TRAPed neurons. MSDB, medial septum and diagonal band of Broca; MEC, medial entorhinal cortex; PVT, paraventricular thalamus; ATN, anterior thalamic nuclei; NR, nucleus reuniens; MRN, median raphe nucleus; LEC, lateral entorhinal cortex. Mice: HC, $n = 4$ and Ext-TRAPed, $n = 5$. Data are presented as means ± SEM. *$P < 0.05$; **$P < 0.01$.

injection express TVA and G and are therefore available for rabies infection and retrograde monosynaptic tracing (Fig. 1B) (*42*). We observed a higher density of Fos-TRAPed neurons in mice exposed to the extinction context compared to those remaining in the home cage, indicating an activation of the vH in the extinction context (Fig. 1C). We then quantified the number of starter neurons that were double-labeled with enhanced green fluorescent protein (EGFP) and tdTomato in the vH, as well as monosynaptically connected presynaptic input neurons, single-labeled with tdTomato, across the whole brain (Fig. 1, C to E). A greater abundance of both starter neurons and total presynaptic input neurons were observed in Ext-TRAPed mice than controls. Furthermore, Ext-TRAPed mice showed higher tdTomato labeling in the amygdala (*43*) and paraventricular thalamus (*44*)—regions linked to emotional valence, as well as the claustrum that may support attentional processes (*45*) and the nucleus reuniens that plays a role in spatial navigation and memory (*46*). Notably, multiple amygdala nuclei were labeled, together accounting for a relatively large fraction of presynaptic input neurons (means ± SD: 9.2 ± 1.2%).

The BLA is known to play a crucial role in the formation of both fear and extinction memories (*35*, *36*), with distinct pyramidal neuron populations oppositely responding to reinforced CS, leading to either the expression or suppression of conditioned fear (*10*). Therefore, we hypothesized that BLA signals arriving at the vH during conditioning may convey stimulus information, allowing for their contextualization (*47*). To test this idea, we performed optogenetic inhibition of BLA glutamatergic terminals in the vH during the CS periods of extinction training. The BLA was infused with AAV to express ArchT or enhance yellow fluorescent protein (EYFP) under the control of the calcium/calmodulin-dependent protein kinase IIα (*CaMKIIα*) promoter (AAV5-CaMKIIα-eArchT3.0-EYFP/-EYFP), and optic fibers were implanted in the vH (Fig. 2A). Before extinction, mice were habituated to auditory cues that were later paired (CS^+) or not paired (CS^-) with electric foot shocks during fear conditioning (Fig. 2B). Subsequently, mice underwent three extinction sessions, with light delivery beginning after the initial trials when freezing began to decline [extinction 1 (Ext 1) from fifth CS^+ and Ext 2 and Ext 3 from third CS^+] (Fig. 2C). Inhibition of BLA projections did not have a direct effect on CS-induced freezing levels during extinction training. However, at the extinction memory test in the absence of light, $ArchT^{BLA\rightarrow vH}$ mice showed higher CS freezing compared to $EYFP^{BLA\rightarrow vH}$, while no differences were observed at fear renewal in the original fear context (Fig. 2D). Since extinction remained intact during training when animals likely use short-term memory of CS outcomes but was impaired at extinction memory test when performance relies on long-term memory, BLA terminal inhibition likely disrupted the formation of a stable well-consolidated long-term extinction memory. To examine whether this manipulation affected contextual fear, we looked at freezing during the acclimation epoch before CS delivery. After light manipulation, $ArchT^{BLA\rightarrow vH}$ mice exhibited higher contextual freezing selectively in the extinction context (Fig. 2E). These data suggest that BLA input during extinction learning may instruct vH representations of cue and contextual safety.

CS-related activity in the vH at extinction memory retrieval

To test whether vH representations depend on the BLA, we recorded the activity of neurons in the vH of mice undergoing fear extinction while inhibiting BLA neurons that project to the vH. To do so, we performed single-unit extracellular electrophysiological recordings with tetrode-loaded microdrives in the vH (Fig. 3A and fig. S1A). Mice expressed either Arch or EYFP in BLA glutamatergic neurons projecting to the vH following unilateral dual infusion of AAV-retro-CaMKIIα-Cre into vH and AAV5-EF1α-DIO-eArch3.0-EYFP/-EYFP into the BLA. Light was delivered via an optic fiber implanted above the BLA. Laser stimulation in the home cage interfered with vH neuronal activity of $Arch^{BLA\rightarrow vH}$ mice ($EYFP^{BLA\rightarrow vH}$: 4 mice, 68 neurons and $Arch^{BLA\rightarrow vH}$: 4 mice, 81 neurons; fig. S1, B to F). To manipulate BLA signals related to extinction, light was delivered during the CS period of extinction training sessions (light on at Ext 1 trials 5 to 12, Ext 2 trials 1 to 24, and Ext 3 trials 1 to 24; Fig. 3B and fig. S2, A to D). Before and after each behavioral session, we recorded offline neuronal activity during rest/sleep periods in the home cage. We analyzed the activity of putative pyramidal neurons in mice with histologically verified tetrode locations in the vH ($EYFP^{BLA\rightarrow vH}$: 179 neurons from 15 mice and $Arch^{BLA\rightarrow vH}$: 185 neurons from 15 mice; Fig 3A and fig. S1, A and E).

To investigate whether the vH responds to the CS during fear extinction, we measured CS-evoked activity across extinction sessions (Fig. 3, C to G). At the population level, we found that trial-averaged normalized CS responses were relatively more excitatory during the extinction memory test compared to extinction training sessions in $EYFP^{BLA\rightarrow vH}$ mice but not in $Arch^{BLA\rightarrow vH}$ mice (Fig. 3C). At extinction memory test, the population firing rate following CS onset was diminished in $Arch^{BLA\rightarrow vH}$ compared to $EYFP^{BLA\rightarrow vH}$ mice (Fig. 3, D and F). We additionally categorized neurons as CS-active or CS-inhibited using a permutation test on the firing rate across the pre-CS and CS periods (see Materials and Methods) and observed that $Arch^{BLA\rightarrow vH}$ mice exhibited a 50% reduction in the proportion of CS-active neurons (11%, 21 of 185 neurons) compared to $EYFP^{BLA\rightarrow vH}$ mice (22%, 39 of 179 neurons) (Fig. 3E). To assess the behavioral relevance of CS-related activity during fear extinction, we correlated CS-induced freezing with CS-related neuronal activity averaged across neurons from Ext 1 to extinction memory test (Fig. 3G). We found a negative association between CS freezing and CS activity in $EYFP^{BLA\rightarrow vH}$ and $Arch^{BLA\rightarrow vH}$ mice, indicating that higher population firing rates during the CS were predictive of lower freezing levels. This finding is consistent with the notion that CS-related activity in the vH at extinction reflects the degree of safety learning.

Reactivation of CS-related activity during extinction consolidation

In the hippocampus, experiences stored in long-term memory must first undergo consolidation, whereby ensemble activity patterns are reactivated, predominantly during slow wave non–rapid eye movement (NREM) sleep (*48*, *49*). To evaluate whether population-level activity patterns during the extinction of the CS reemerge in NREM sleep, we examined the similarity of pairwise correlations between all pyramidal neurons obtained during extinction learning sessions and those immediately following the session during offline NREM sleep (post-NREM) (Fig. 3A). Activity occurring during offline NREM sleep immediately before each extinction learning session (pre-NREM) served as baseline. In the $EYFP^{BLA\rightarrow vH}$ group, a positive association between CS and post-NREM correlations was observed, which was greater than the association between CS and

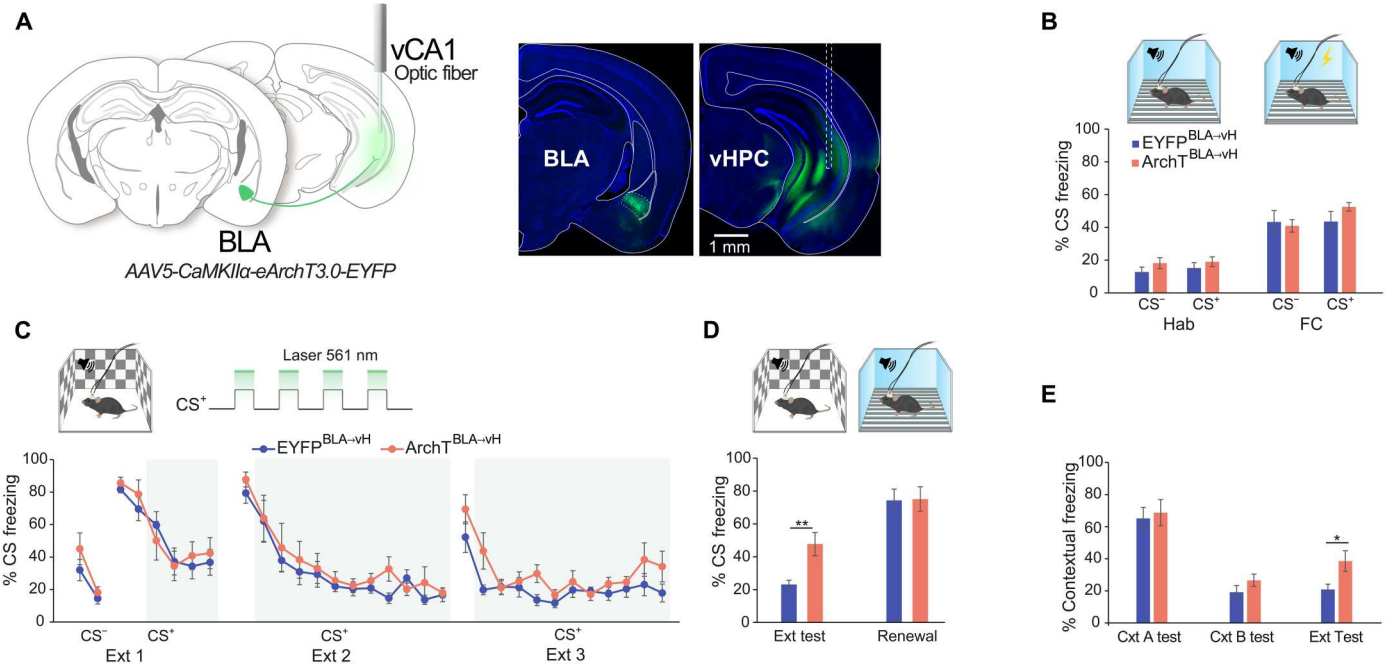

Fig. 2. BLA inputs to the vH facilitate fear extinction memory formation. (**A**) Left: Schematic of optogenetic BLA-vH terminal inhibition strategy showing vH optic fiber implantation and BLA viral transduction. Right: Representative images of eArchT3.0 expression in the BLA and vH. Dashed lines indicate optic fiber track. vHPC, ventral hippocampus. (**B**) Percentage of conditioned stimuli (CS) period freezing in four-trial averaged blocks during habituation (Hab) and fear conditioning (FC) sessions in context A (top illustration). Hab: CS^-, $t_{(13)} = 1.2$, $P = 0.25$; CS^+, $t_{(13)} = 0.85$, $P = 0.41$. FC: CS^-, $t_{(13)} = 0.29$, $P = 0.77$; CS^+, $t_{(13)} = 1.28$, $P = 0.4$, unpaired *t* tests. (**C**) Top: Context B illustration and paradigm for laser light delivery during the CS period of Ext sessions. Percent CS freezing across Ext training sessions shown as two-trial averaged blocks. Shaded area indicates light-on trial blocks. Ext 1, $F_{7,91} = 0.67$, $P = 0.7$; Ext 2, $F_{11,143} = 0.64$, $P = 0.79$; Ext 3, $F_{11,143} = 1.23$, $P = 0.27$, two-way repeated measures (RM) analysis of variance (ANOVA) per session, time × group interaction. (**D**) Percent CS period freezing in four-trial averaged blocks at Ext test and fear renewal test (renewal) in contexts B and A (top). Ext test: $t_{(13)} = 3.54$, $P = 0.004$; renewal: $t_{(13)} = 0.1$, $P = 0.92$, unpaired *t* tests. (**E**) Percent contextual freezing during first 3 min of context exposure in each session. Context A test (contextual fear memory test): $t_{(13)} = 0.34$, $P = 0.74$; context B test (novel context fear discrimination test): $t_{(13)} = 1.3$, $P = 0.22$; Ext test (extinction memory test in context B): $t_{(13)} = 2.55$, $P = 0.024$, unpaired *t* tests. Mice: $EYFP^{BLA\rightarrow vH}$, $n = 8$ and $ArchT^{BLA\rightarrow vH}$, $n = 7$. Data are presented as means ± SEM. $^*P < 0.05$; $^{**}P < 0.01$.

pre-NREM correlations. In contrast, no difference between post- and pre-NREM associations was observed in the $Arch^{BLA\rightarrow vH}$ group. We then examined the explained variance of CS-related activity; i.e., the percentage of variance in the pairwise correlations obtained during CS presentations predicted from the set that was obtained during sleep (Fig. 4, B to D) (*50*). We found that post-NREM activity accounted for a higher percentage of variance in CS-related activity compared to pre-NREM at extinction sessions 1, 2, and 3 in the $EYFP^{BLA\rightarrow vH}$ group, whereas a difference was found only at Ext 1 in the $Arch^{BLA\rightarrow vH}$ group (Fig. 4B). Furthermore, the $Arch^{BLA\rightarrow vH}$ group had lower post-NREM explained variance than the $EYFP^{BLA\rightarrow vH}$ group at each extinction training session once laser light was delivered (Fig. 4C). Moreover, we examined whether the reactivation of CS-active neurons was disrupted in the $Arch^{BLA\rightarrow vH}$ group and noticed a reduction in post-NREM explained variance at Ext 1 and 2 (Fig. 4D). Similar findings were also observed for REM sleep (fig. S3, A to D). This suggests that CS-related activity in vH during extinction learning is reactivated during sleep for extinction memory consolidation.

Fear and extinction memory retrieval is known to involve the synchronization of theta frequency local field potential oscillations (4 to 12 Hz) between the amygdala and hippocampus (*51*, *52*). We examined local field potentials in the vH triggered by CS presentation across extinction sessions. CS-evoked power was most prominent in the 3- to 8-Hz frequency range (Fig. 5, A and B), emerged after fear conditioning, declined during extinction training, and rebounded at the extinction memory test (fig. S3E). The timing of spiking activity of hippocampal neurons is coordinated by local theta oscillations, with spikes of different neurons occurring at preferred phases of the theta cycle (*53*). Thus, we analyzed the spike-phase coupling of CS-active neurons during the extinction memory test (Fig. 5, C to E) and observed that a substantial fraction of these neurons were significantly coupled to theta oscillations during the CS ($EYFP^{BLA\rightarrow vH}$: 68% and $Arch^{BLA\rightarrow vH}$: 55%) relative to the pre-CS period ($EYFP^{BLA\rightarrow vH}$: 43% and $Arch^{BLA\rightarrow vH}$: 40%) (Fig. 5D). As a population, the spikes of significantly phase-locked neurons predominantly occurred at the trough of the theta cycle for both $EYFP^{BLA\rightarrow vH}$ and $Arch^{BLA\rightarrow vH}$ groups (Fig. 5C). Of particular note, CS-active neurons from $Arch^{BLA\rightarrow vH}$ mice showed diminished strength of theta coupling compared to those from $EYFP^{BLA\rightarrow vH}$ mice not only during the CS but also during the pre-CS period when the context may prime cue associations (Fig. 5E). This decrease in theta coupling was not detected in early extinction sessions but emerged at extinction 3 (fig. S3F).

Spatial representation of the extinction context

The vH contains neurons with broad spatial firing fields that map onto affective zones within an arena (*25*, *54*, *55*). To explore the spatial representation of the extinction context by vH neurons, we examined the most prominent features of spatial firing fields using

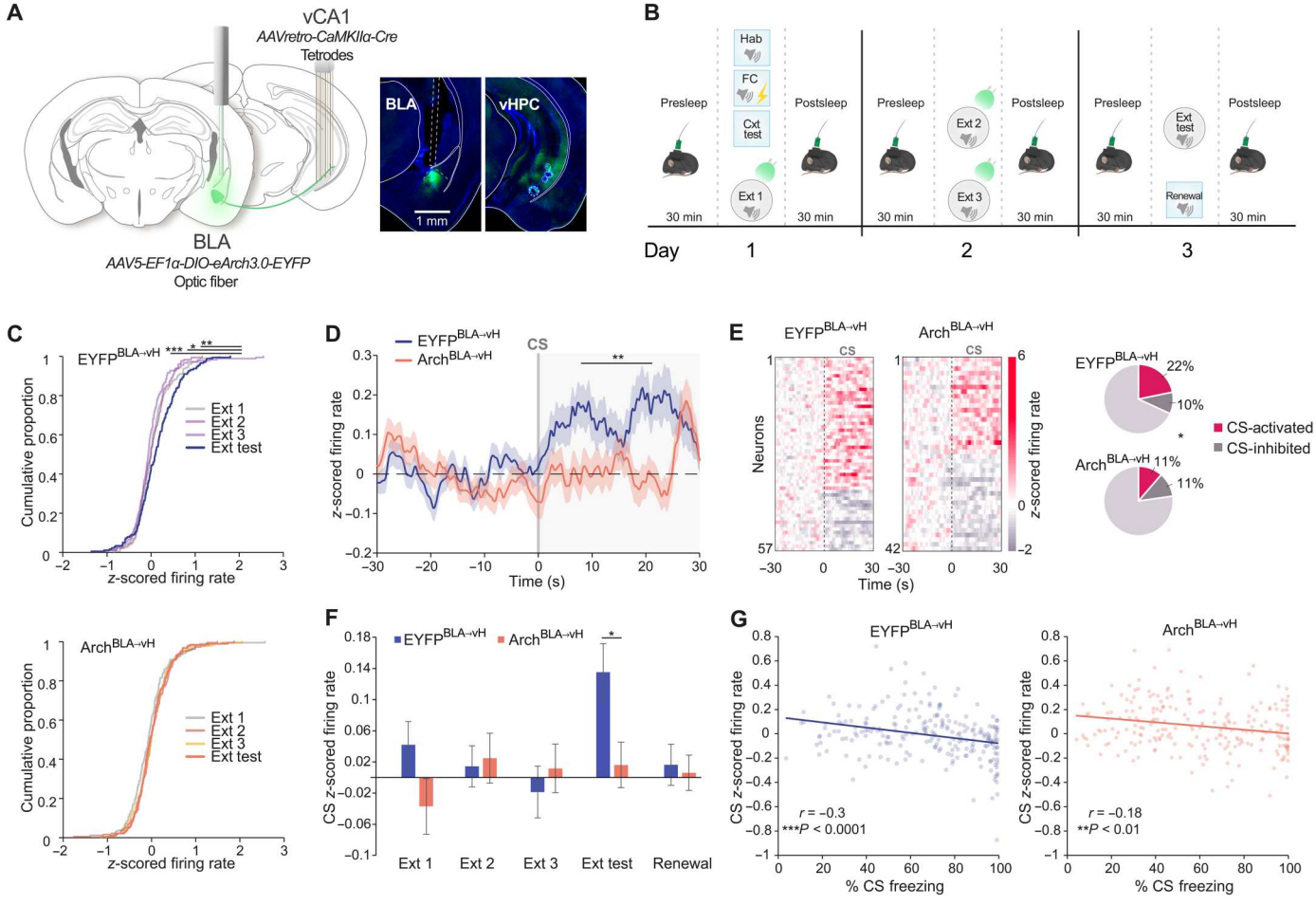

Fig. 3. BLA-vH circuit inhibition at extinction learning disrupts CS-evoked activity at extinction memory retrieval. (**A**) Left: Schematic of electrophysiological recordings from vH and optogenetic somatic inhibition of BLA→vH neurons. Right: Representative eArch3.0 expression in BLA and vH. Tetrode positions in vH stratum pyramidale. (**B**) Paradigm for electrophysiological recordings, optogenetics, and behavior. Light delivery during CS period of Ext training sessions. (**C**) Cumulative proportion of neurons with given mean normalized firing rate during CS at Ext sessions (mean of first four CS trials in each session; top, $EYFP^{BLA\rightarrow vH}$ and bottom, $Arch^{BLA\rightarrow vH}$). $EYFP^{BLA\rightarrow vH}$: Ext 1, $D_{(179)} = 0.19$, $P = 0.0043$; Ext 2, $D_{(179)} = 0.17$, $P = 0.0106$; Ext 3, $D_{(179)} = 0.25$, $P < 0.0001$. $Arch^{BLA\rightarrow vH}$: Ext 1, $D_{(185)} = 0.11$, $P = 0.23$; Ext 2, $D_{(185)} = 0.07$, $P = 0.74$; Ext, 3 $D_{(185)} = 0.05$, $P = 0.98$, Kolmogorov-Smirnov test against Ext Test. (**D**) Population trial-averaged normalized firing rate time-locked to CS onset at Ext test. Group effect: $F_{1,361} = 6.71$, $P = 0.01$; time × group interaction: $F_{149,53789} = 2.26$, $P < 0.0001$, two-way RM ANOVA for CS period. (**E**) Left: Peri-stimulus time histogram heatmaps of activated and inhibited neuronal responses to the CS. Right: Percent CS-active and CS-inhibited pyramidal neurons. Count differences of CS-active, CS-inhibited, and nonresponsive neurons between groups: $\chi^2_{(2,\,N\,=\,364)} = 7.2$, $P = 0.027$, chi-square test. (**F**) Mean population normalized firing rates during CS period (mean of first four CS trials in each session). Ext test: $t_{(361)} = 2.56$, $P = 0.011$, unpaired t test. (**G**) Correlation between mean normalized firing rate and percent freezing during CS. Data points show four-trial averaged blocks from Ext 1 to Ext test per mouse. Lines show least squares linear fits ($EYFP^{BLA\rightarrow vH}$, $r = -0.30$, $P < 0.0001$; $Arch^{BLA\rightarrow vH}$, $r = -0.18$, $P = 0.0076$, Pearson's r). $EYFP^{BLA\rightarrow vH}$: $n = 179$ neurons from 15 mice and $Arch^{BLA\rightarrow vH}$: $n = 185$ neurons from 15 mice. *$P < 0.05$; **$P < 0.01$; ***$P < 0.0001$.

principal components analysis, where pixels of the context served as dimensions and neurons as instances. For both $EYFP^{BLA\rightarrow vH}$ and $Arch^{BLA\rightarrow vH}$ groups, the first 10 components captured approximately 80% of the variance, and inspection of eigenvector maps revealed variation in the center activity to be the most dominant feature (fig. S4E).

The center may be considered as aversive relative to the periphery, which has protective sidewalls, as evidenced by the strong avoidance for the center zone of the extinction context (fig. S4, A to D). We categorized neurons as center-active (center neurons) or center-inhibited (periphery neurons) in the extinction context at the extinction memory test (see Materials and Methods, Fig. 6A, and fig. S4F). Whereas the $EYFP^{BLA\rightarrow vH}$ group exhibited a higher proportion of periphery neurons compared to center neurons, the $Arch^{BLA\rightarrow vH}$ group showed the opposite pattern with more center than periphery neurons (Fig. 6B,C). This was also observed when taking the ratio of periphery-to-center cell counts in individual mice (Fig. 6C). These findings were not explained by differences in speed in each zone or by the abundance of speed-modulated neurons (fig. S5, A to D). Since contextual representations are theorized to gate CS associations, we examined whether the proportions of zone neurons may be related to CS-induced freezing. In the $EYFP^{BLA\rightarrow vH}$ group, mice with more neurons coding the periphery relative to the center exhibited lower CS-related freezing, suggesting that biased representation of the periphery predicted stronger extinction memory retrieval (Fig. 6D). We then compared the

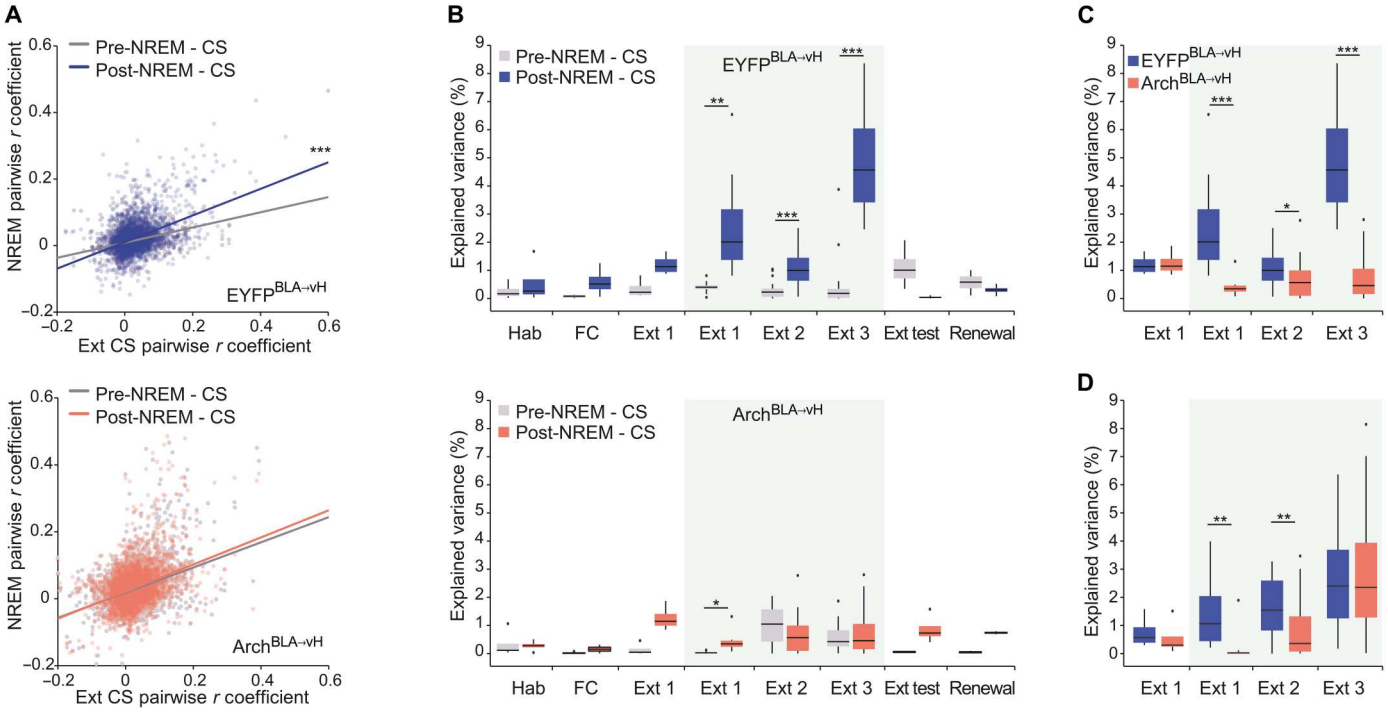

Fig. 4. BLA-vH inhibition at extinction learning impairs the reactivation of CS-related activity during sleep. (**A**) Pairwise correlations for the CS period activity at Ext sessions versus for pre-NREM (non–rapid eye movement) or post-NREM sleep (top: $EYFP^{BLA\rightarrow vH}$, $n = 179$ neurons from 15 mice; bottom: $Arch^{BLA\rightarrow vH}$, $n = 185$ neurons from 15 mice). $EYFP^{BLA\rightarrow vH}$: $n = 3501$ pairs, pre–NREM-CS, $r = 0.36$, $P = 8.9 \times 10^{-110}$; post–NREM-CS, $r = 0.45$, $P = 3.7 \times 10^{-176}$; $Arch^{BLA\rightarrow vH}$: $n = 4295$ pairs, pre–NREM-CS, $r = 0.37$, $P = 1.9 \times 10^{-139}$; post–NREM-CS, $r = 0.38$, $P = 1.2 \times 10^{-145}$, Pearson's r. Pre–NREM-CS versus post–NREM-CS: $EYFP^{BLA\rightarrow vH}$, $z = -7.58$, $P = 0$; $Arch^{BLA\rightarrow vH}$, $z = -0.91$, $P = 0.36$, Steiger's z test. (**B**) Explained variance of pairwise correlations between CS and pre-NREM versus CS and post-NREM (top: $EYFP^{BLA\rightarrow vH}$ and bottom: $Arch^{BLA\rightarrow vH}$). $EYFP^{BLA\rightarrow vH}$: Ext 1 light trials, $P = 0.0078$; Ext 2, $P = 0.0003$; Ext 3, $P < 0.00001$; $Arch^{BLA\rightarrow vH}$: Ext 1 light trials, $P = 0.0156$; Ext 2: $P = 0.14$; Ext 3, $P = 0.73$, Wilcoxon signed-rank test. (**C**) Explained variance of pairwise correlations between CS and post-NREM comparing $EYFP^{BLA\rightarrow vH}$ versus $Arch^{BLA\rightarrow vH}$. Ext 1 light trials: $P = 0.0006$, Ext 2: $P = 0.0303$, Ext 3: $P < 0.00001$, Wilcoxon rank sum test. (**D**) For CS-active neurons, explained variance of pairwise correlations between CS and post-NREM comparing $EYFP^{BLA\rightarrow vH}$ versus $Arch^{BLA\rightarrow vH}$. Ext 1 light trials, $P = 0.003$; Ext 2, $P = 0.0067$; Ext 3, $P = 0.41$. $EYFP^{BLA\rightarrow vH}$, $n = 39$ neurons and $Arch^{BLA\rightarrow vH}$, $n = 21$ neurons. $^*P < 0.05$; $^{**}P < 0.01$; $^{***}P < 0.001$.

spatial properties of periphery and center neurons between $EYFP^{BLA\rightarrow vH}$ and $Arch^{BLA\rightarrow vH}$ groups. We found poorer selectivity for the periphery zone and larger spatial fields among periphery neurons in the $Arch^{BLA\rightarrow vH}$ group (Fig. 6, E and F). Furthermore, the spiking activity of periphery neurons in both groups showed higher information content for spatial position in the extinction context than that of center neurons, consistent with the notion that center activity can also reflect a nonspatial and perhaps emotional component of the context (Fig. 6G). Furthermore, periphery neurons of $Arch^{BLA\rightarrow vH}$ mice carried less spatial information than those of $EYFP^{BLA\rightarrow vH}$ mice.

Precise spatial coding of the extinction context may facilitate the retrieval of CS representations during extinction. In the $EYFP^{BLA\rightarrow vH}$ group, we observed that a more distinct coding of the periphery zone was associated with an increased population activity during the CS (Fig. 6H). Similarly, CS-related activity was larger with more restricted place field sizes (Fig. 6I) and with a trend for higher spatial information (fig. S5G). As with CS-active neurons, a large fraction of periphery and center neurons fired phase-locked to the local theta oscillation in both groups (fig. S5E). However, while periphery neurons in the $EYFP^{BLA\rightarrow vH}$ group showed stronger coupling than center neurons, no difference was seen in the $Arch^{BLA\rightarrow vH}$ group (fig. S5F). Given the ability of vH neurons to discriminate zones, we determined whether the position of mice in the periphery or center could be decoded from their activity. For individual mice, we trained a linear classifier (support vector machine) on the firing rate of pyramidal neurons in time during trajectories from the periphery into the center (Fig. 7, A and B). The test classification accuracy was above chance level for both groups; however, there was a decrease in the test accuracy for $Arch^{BLA\rightarrow vH}$ compared to $EYFP^{BLA\rightarrow vH}$ mice (Fig. 7B), indicating less distinct activity patterns in the periphery and center zones for $Arch^{BLA\rightarrow vH}$ mice. Since spikes of neurons in the $Arch^{BLA\rightarrow vH}$ group carried less information regarding spatial location, we evaluated whether the animal's position could be reconstructed from spiking activity. Using a Bayesian decoder (*55*–*57*), we found that the spatial location was predicted with lower accuracy in $Arch^{BLA\rightarrow vH}$ mice compared to $EYFP^{BLA\rightarrow vH}$ mice, with a decoding accuracy significantly above chance level for both groups as assessed with shuffled labels (Fig. 7, C and D).

Together, these findings suggest that periphery neurons convey more precise spatial information about the context, which may aid retrieval of the associated cued extinction memory. Because $Arch^{BLA\rightarrow vH}$ mice exhibited dysfunctional periphery and enhanced center activity, these alterations may result in poorer spatial processing leading to impaired extinction memory retrieval.

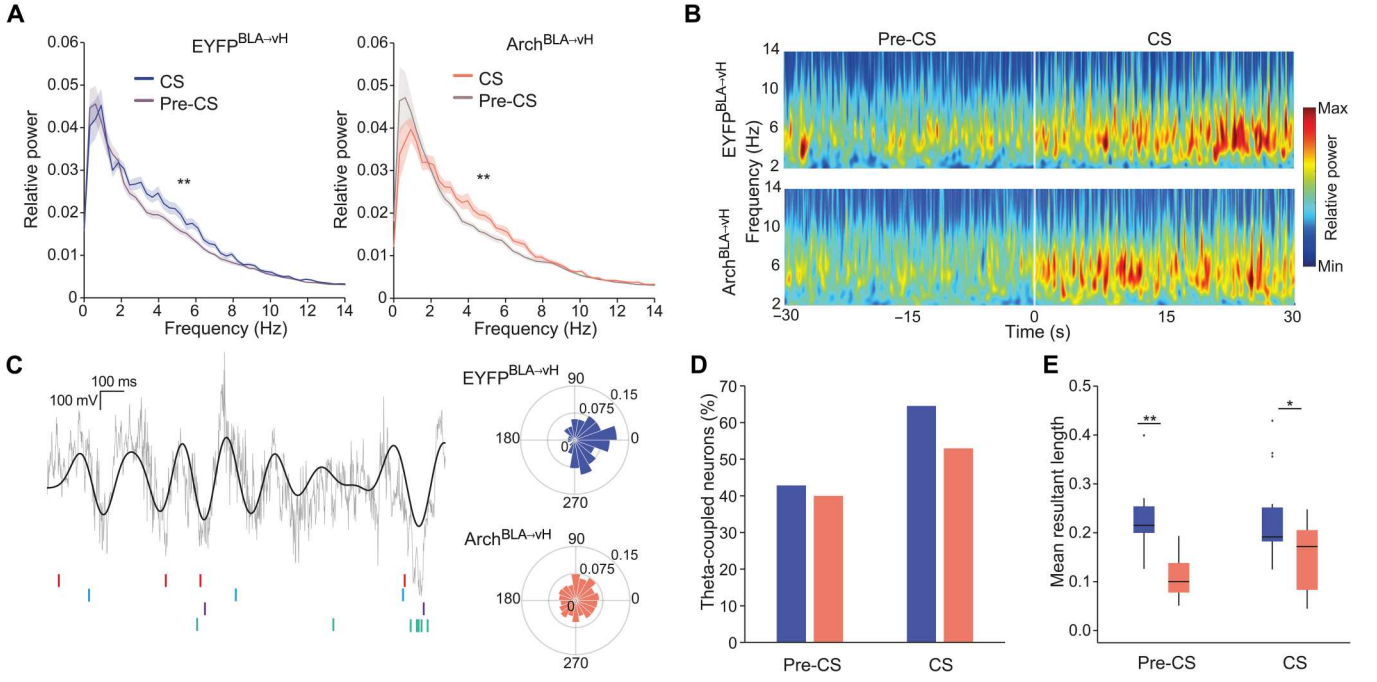

Fig. 5. BLA-vH inhibition at extinction learning weakens vH neuronal synchronization to local theta oscillations at extinction memory retrieval. (**A**) Power spectral density estimates at Ext test pre-CS and CS periods. Power normalized to total power pre-CS. Left, EYFP$^{BLA\rightarrow vH}$ ($F_{1,28}$ = 8.25, P = 0.0077, n = 15 mice); right, Arch$^{BLA\rightarrow vH}$ ($F_{1,28}$ = 7.87, P = 0.009, n = 15 mice), two-way RM ANOVA 3- to 8-Hz epoch effect. (**B**) Spectrogram of CS-triggered local field potential (LFP) power at Ext test averaged across trials and mice (n = 15 each group). (**C**) Left: Representative traces from an EYFP$^{BLA\rightarrow vH}$ mouse of raw and filtered (4- to 12-Hz) LFP, with spikes from four theta-coupled CS-active neurons shown below. Right: Example polar histograms of spike phase angles of CS-active theta-coupled neurons. EYFP$^{BLA\rightarrow vH}$ neuron: mean angle = 354°, mean resultant vector length (MRL) = 0.36, P = 0.001; Arch$^{BLA\rightarrow vH}$ neuron: mean angle = 31°, MRL = 0.08, P = 0.0455, Rayleigh's test. (**D**) Percent CS-active neurons significantly coupled to theta (4 to 12 Hz) during pre-CS and CS periods. Pre-CS: EYFP$^{BLA\rightarrow vH}$, n = 9 of 21 neurons; Arch$^{BLA\rightarrow vH}$, n = 6 of 15 neurons; CS: EYFP$^{BLA\rightarrow vH}$, n = 20 of 31 neurons, Arch$^{BLA\rightarrow vH}$: n = 9 of 17 neurons. (**E**) MRL of theta-coupled CS-active neurons. Pre-CS, P = 0.0028; CS, P = 0.03, Wilcoxon rank sum test.

DISCUSSION

Because animals seek resources to fulfill biological needs, they must adapt their behavior to the various environments encountered. Among the assortment of memories stored in neuronal networks throughout the brain, associations appropriate to specific contexts need to be selected to guide responding (*58*). We have shown that the vH plays a fundamental role in context-dependent extinction memory selection. The vH simultaneously forms a safety CS and context representation, orchestrated by the BLA, which promotes retrieval of fear extinction over fear memory.

We found that vH neurons activated in the extinction context are monosynaptically innervated by the BLA. During extinction learning, this circuit supported CS-related activity patterns in the vH that reactivated during sleep, allowing for the emergence of an extinction CS safety signal synchronized to theta oscillations. CS-related activity was primed by a representation of the extinction context where safe zones were preferentially represented and with higher spatial fidelity. This finding implies that CS-related valence is translated into an affectively congruent and precise spatial representation in the vH (14) .

A large body of work has implicated the amygdala in assigning valence to sensory cues and the environment (*59*–*61*), which consequently informs the animal's affective behavioral state (*61*–*65*). BLA projections to the vH, specifically from the posterior portion of the BLA, appear to promote exploration of anxiogenic zones (*38*). Furthermore, BLA pyramidal neurons projecting to the vH have been found to code for CS associated with natural reward (*39*). BLA neurons activated by reward partially overlap with those active during extinction memory retrieval (*14*). This finding is consistent with the hypothesis that extinction involves negative reinforcement learning where omission of the aversive US elicits a dopamine-mediated reward prediction error signal that reinforces the suppression of conditioned fear responses (*66*–*69*). During extinction learning, BLA glutamatergic inputs to the vH may convey an instructive signal of CS valence (*70*), inducing the formation of safety representations in the vH. Once consolidated, these safety associations may be retrieved and conveyed to remote downstream structures such as the amygdala, infralimbic cortex, and nucleus accumbens (*28*, *33*, *69*), via synchronized theta oscillations for long-range communication (*71*, *72*). However, future studies should be conducted to investigate extinction-related neuronal representations in BLA neurons that project to the vH.

A limitation of the current study is that optogenetic inhibition of the BLA-vH circuit during electrophysiological recordings was conducted by means of somatic inhibition of BLA neurons that project to the vH. This approach was taken to avoid photovoltaic artifacts in the electrophysiological recordings (*73*, *74*, *75*). While we demonstrated that BLA-vH somatic inhibition impaired extinction memory to a similar extent as BLA-vH terminal inhibition, we cannot rule out the possibility that BLA neurons projecting to the vH may send axon collaterals to other brain structures that, in turn, innervate the vH and contribute to the neural activity patterns

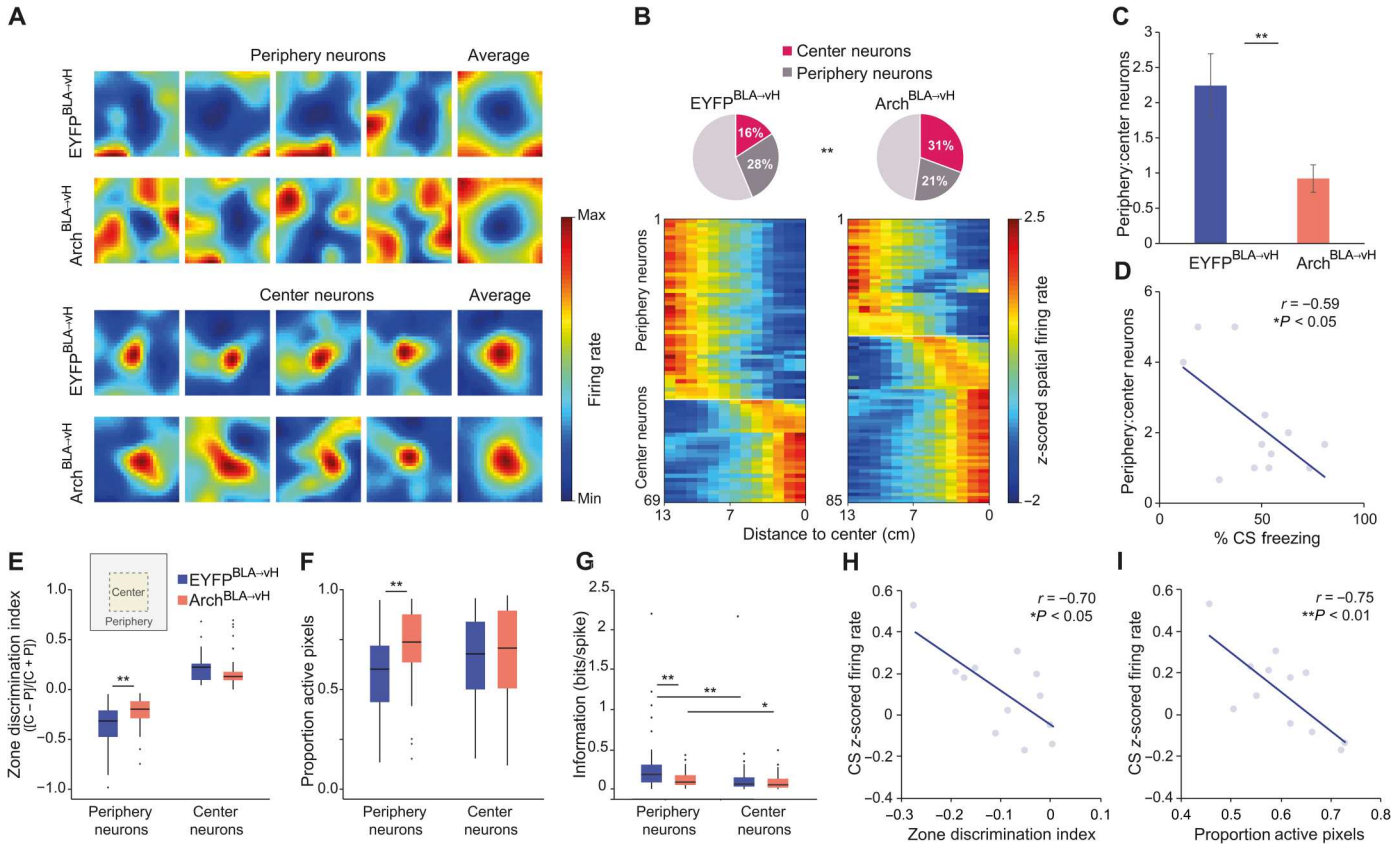

Fig. 6. BLA-vH inhibition during extinction learning alters vH zone representations within the extinction context. (**A**) Representative spatial firing rate maps at Ext test of periphery and center neurons. Population averaged maps in each category shown at the right end. (**B**) Top: Percent of periphery and center neurons. Count differences of periphery, center, and nonzone neurons between groups: $\chi^2_{(2,\ N\ =\ 321)} = 10.01$, $P = 0.0067$, chi-square test. Bottom: Linearized spatial firing rate maps for periphery and center neurons. (A and B) EYFP$^{BLA\rightarrow vH}$, $n = 158$ neurons from 15 mice and Arch$^{BLA\rightarrow vH}$, $n = 163$ neurons from 15 mice. (**C**) Count ratios of periphery and center neurons per mouse. $t_{(24)} = 2.83$, $P = 0.0094$. EYFP$^{BLA\rightarrow vH}$, $n = 12$ mice and Arch$^{BLA\rightarrow vH}$, $n = 14$ mice, unpaired t test. Data presented as means ± SEM. (**D**) Ratio of periphery and center cell counts against percent CS freezing at Ext test per EYFP$^{BLA\rightarrow vH}$ mouse ($n = 12$). $r = -0.59$, $P = 0.0425$, Pearson's r. (**E**) Zone discrimination index of periphery (P) and center (C) neurons calculated with mean firing rates in each zone. Periphery neurons, $P = 0.0039$; center neurons, $P = 0.20$, Wilcoxon rank sum test. (**F**) Proportion of total active maze pixels. Periphery neurons, $P = 0.0016$; center neurons, $P = 0.39$, Wilcoxon rank sum test. (**G**) Spatial information content of spiking activity. Periphery neurons, $P = 0.0099$; center neurons, $P = 0.35$; EYFP$^{BLA\rightarrow vH}$, $P = 0.0042$; Arch$^{BLA\rightarrow vH}$, $P = 0.0285$, Wilcoxon rank sum test. (D to G) Periphery neurons: EYFP$^{BLA\rightarrow vH}$, $n = 44$; Arch$^{BLA\rightarrow vH}$, $n = 35$; center neurons: EYFP$^{BLA\rightarrow vH}$, $n = 25$; Arch$^{BLA\rightarrow vH}$, $n = 50$. (**H**) Zone discrimination index against mean normalized firing rates during CS period. $r = -0.70$, $P = 0.012$. (**I**) Proportion of active maze pixels against mean normalized CS firing rate. $r = -0.75$, $P = 0.0053$, Pearson's r. (H and I) Measures averaged across all neurons from individual EYFP$^{BLA\rightarrow vH}$ mice ($n = 12$) at Ext test.

observed. Structures that receive inputs from the BLA and that send outputs to the vH include the lateral entorhinal cortex, medial preoptic area, and claustrum (*76*). In particular, studies in rats suggest a potential role of the entorhinal cortex in fear extinction and renewal (*77*, *78*, *79*). Thus, future studies should evaluate the function of entorhinal cortical projections to the vH in these behaviors.

A classical view posits that to retrieve context-dependent cue associations, the hippocampus transmits contextual information to downstream areas involved in the encoding of discrete cues (*3*). However, we found that context gating can arise locally within the vH where spatial activity facilitates cue responses. This finding supports a contextual binding model in which the hippocampus encodes an episodic memory of items along with the specific context where they were encountered (*80*). Evidence from human studies suggest that explicit memory of the context and CS—no-US association may be formed in the vH, while the CS—no-US association may be stored as an implicit memory in the amygdala eliciting conditioned suppression of fear responses (*81*, *82*).

The vH contains functionally heterogeneous populations of neurons defined by their distinct projection targets and molecular profiles (*24*, *83*–*85*). Although the present study did not characterize the projection targets of recorded vH neurons, it is plausible that the distinct neuronal activity patterns observed are performed by anatomically segregated neuronal populations. A previous study reported that center-active neurons were enriched among vH neurons projecting to the lateral hypothalamus, which served to promote anxiety-related behaviors (*28*). We found that vH neurons also discriminate center and periphery zones in a context with acquired valence. The proportion of vH neurons that we observed with preferential activity in the center of the extinction context (16%) was highly similar to the reported proportion of center-active neurons in the open field test (17%) (*28*). Meanwhile, the vH neurons that we observed with place fields selectively located

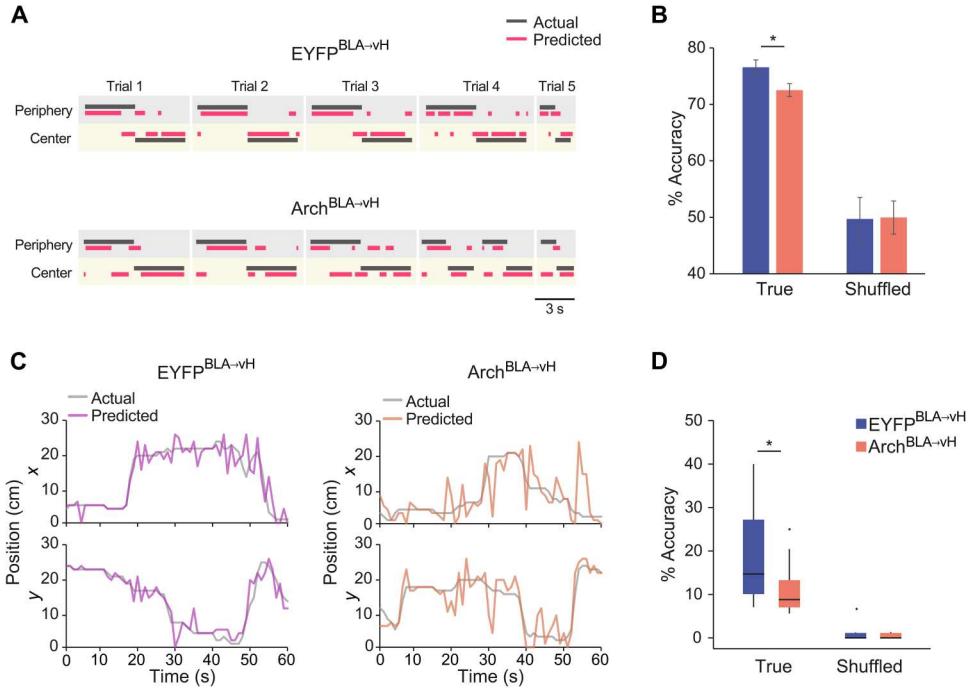

Fig. 7. BLA-vH inhibition during extinction learning diminishes vH spatial coding of the extinction context. (**A**) Zone decoding accuracy using a support vector machine classifier (SVM) with representative zone decoding from an EYFP$^{BLA→vH}$ and Arch$^{BLA→vH}$ mouse showing actual and predicted zone location for individual periphery-center trajectories. (**B**) Percent correct zone classification using SVM models trained with true or shuffled labels. EYFP$^{BLA→vH}$ versus Arch$^{BLA→vH}$, $z = 2.30$, $P = 0.021$, z test. True versus shuffled, EYFP$^{BLA→vH}$, $z = 6.64$, $P < 0.00001$; Arch$^{BLA→vH}$, $z = 7.13$, $P < 0.00001$, z test. EYFP$^{BLA→vH}$, $n = 9$ mice and Arch$^{BLA→vH}$, $n = 12$ mice. Data are presented as means ± SD. (**C**) Representative positional decoding using a Bayesian decoder from an EYFP$^{BLA→vH}$ and Arch$^{BLA→vH}$ mouse showing actual and predicted x and y locations across time. (**D**) Percent correct Bayesian decoding of location using models trained with true or shuffled labels. EYFP$^{BLA→vH}$ versus Arch$^{BLA→vH}$, $P = 0.026$, Wilcoxon rank sum test. True versus shuffled, EYFP$^{BLA→vH}$, $P = 0.00012$; Arch$^{BLA→vH}$, $P = 0.00012$, Wilcoxon signed-rank test. EYFP$^{BLA→vH}$, $n = 14$ mice and Arch$^{BLA→vH}$, $n = 14$ mice.

in the periphery zone may also be involved in encoding spatial and affective contextual features. These neurons may belong to a population that is functionally and anatomically distinct from center-active neurons, an area that should be explored in future studies. BLA glutamatergic inputs have been found to form synapses selectively onto BLA and nucleus accumbens projecting neurons in the vH (*86*). Notably, projections from the vH to the nucleus accumbens are known to play an important role in associating context with various forms of rewards (*24*, *31*, *87*, *88*) and may therefore contribute to the safety-related neuronal representations observed during extinction memory retrieval (*69*). In contrast, vH neurons that project to the central amygdala and infralimbic cortex have been implicated in the facilitation of fear renewal after extinction (*27*, *33*). BLA-vH terminal inhibition during extinction did not alter CS freezing at fear renewal, suggesting that vH neurons supporting fear renewal were not affected. Future studies are needed to understand the mechanisms by which context influences the activity of identified vH neuronal populations to gate the retrieval of fear and extinction memories.

Extinction memory involves the coactivity of distributed neuronal populations, forming a functional network to counter aversive states (*9*, *61*). We discovered that BLA signals arriving at the vH during fear extinction learning led to the formation of vH neuronal representations of contextual and CS safety that support extinction memory retrieval. Our findings provide insight into how dysfunctional interactions between the amygdala and hippocampus may impair extinction learning, leading to persistent fear, as seen in anxiety disorders (*89*–*91*).

MATERIALS AND METHODS

Subjects

Mice aged 3 to 4 months were group housed with ad libitum access to food and water in a temperature-controlled room on a 12-hour light/dark cycle. For electrophysiological and optogenetics experiments, male C57BL6/J mice were used (Janvier Labs, France). TRAP2 mice were obtained from the Jackson Laboratory (*Fos*$^{tm2.1(icre/ERT2)Luo}$*/J*, JAX no. 030323), and both male and female homozygous mice were used for experiments. Before surgery and behavioral experiments, mice were gently handled in the home cage for 5 min on three consecutive days to acclimatize them to subsequent procedures. Following surgery, mice undergoing electrophysiological experiments were single-housed. For optogenetics-only and TRAP experiments, littermates were randomly assigned to experimental conditions and group-housed with two to three mice per cage. All experimental procedures were performed in accordance with the guidelines of the Animal Welfare Office at the University of Bern and approved by the Veterinary Office of the Canton of Bern.

Surgical procedures

Mice were anesthetized with isoflurane (induction: 5%, maintenance: 1 to 2% in oxygen at a flow rate of 1 liter/min), and body temperature was maintained at 37°C with a temperature controller (Harvard Apparatus). Analgesia was administered upon induction and for 3 days after operation (carprofen, 2 to 5 mg/kg sc). After mice were mounted onto a stereotaxic frame, the scalp was incised, and craniotomies were made over target regions. Implants were secured to the skull using light-cured dental adhesive (Kerr, OptiBond Universal) and dental cement (Ivoclar, Tetric EvoFlow).

Virus injection and fiber implantation

Viral solution (150 to 300 nl) was delivered via a glass micropipette (30- to 40-μm tip) attached by tubing to a Picospritzer III microinjection system (Parker Hannifin Corporation) at a rate of 100 nl/min. The pipette was left in place for 10 min after infusion to prevent solution backflow. Viral infusions in the vH were performed with the following coordinates: anterior-posterior (AP), −2.90 mm; medial-lateral (ML), ±2.35 mm; dorsal-ventral (DV), −4.95 mm at a 10° lateral angle. For BLA infusions, the coordinates were: AP, −1.5 mm; ML, ±3.3 mm; and DV, −5.1 mm. TRAP2 mice received two viral injections in the right vH. First, AAV2/9-hSyn1-DIO-TVA950-2A-EGFP-2A-oG (ETH Zurich Viral Vector Facility) was infused, which was followed 3 weeks later by *EnvA-N2C-RVdG-tdTomato* (Kavli Institute for Systems Neuroscience Viral Vector Core, Norwegian University of Science and Technology). For optogenetics-only experiments, mice were infused bilaterally in the BLA with either AAV2/5-CaMKIIα-eArchT3.0-EYFP or AAV2/5-CaMKIIα-EYFP (University of North Carolina Vector Core), and optic fibers [200 μm core, 0.37 numerical aperture (NA); Thorlabs] were implanted above the vH at the following coordinates: AP, −2.9 mm; ML, ±3.8 mm; and DV, −3.5 mm. For electrophysiology experiments, mice were infused in the right vH with AAV2-retro-CaMKIIα-iCre (ETH Zurich Viral Vector Facility) and in the right BLA with either AAV2/5-EF1α-DIO-eArch3.0-EYFP or AAV2/5-EF1α-DIO-EYFP (UNC Vector Core). Two weeks later, they were implanted in the right hemisphere with a tetrode microdrive in the vH and optic fiber in the BLA at the following coordinates: AP, −1.7 mm; ML, ±3.3 mm; and DV, −5.0 mm. Only mice with verified transgene expression and/or optic fiber placements in the target sites were included in experimental analyses.

Surgery for in vivo electrophysiology

Mice were implanted with a custom-made microdrive (Axona Ltd.) containing eight independently moveable tetrodes constructed from tungsten wire (12.7 μm; California Fine Wire Company). Tetrode tips were gold-plated to an impedance of 100 to 200 kilohms. The tetrode-loaded microdrive and optic fiber were gradually lowered to their target regions, and craniotomies were sealed with sterile wax. Miniature stainless steel screws (J.I. Morris, F000120CE094) were secured to each hemisphere above the cerebellum and connected to the microdrive's electrode interface board to serve as ground and reference. To detect electromyogram (EMG) activity, paraformaldehyde-coated stainless steel wires (A-M Systems, 791000) were placed in left and right neck muscles.

Behavior

Fear conditioning and extinction

Fear conditioning and extinction took place in two separate arenas both measuring 26 by 26 cm^2 (contexts A and B within sound-attenuating chambers). These contexts were designed to be highly distinct, differing in their floor textures, wall patterns, distal landmarks, and scents (cleaning with either 70% ethanol or 1% acetic acid). At the beginning of each training and test session, mice were acclimated to the arena for 10 min. The auditory cues were pips (7.5 kHz tone for CS^+ and white noise for CS^- at a sound pressure level of 73 dB) lasting 50 ms and repeated every second for a total of 30 pips in 30 s. CS presentations occurred at an intertrial-interval ranging from 30 to 90 s with a mean of 60 s. On day 1, mice were placed in context A and allowed to habituate to the auditory cues through four presentations each of the CS^- followed by the CS^+. Two hours later, they were again placed in context A and subjected to discriminative delay fear conditioning by pairing the CS^+ with an electrical foot shock (US, 1 s, 0.5-mA current, coterminating with the onset of the final pip). CS^- trials were alternated with CS^+—US trials for a total of four trials of each type. Four hours later, mice were tested for contextual fear memory by returning them to context A for 5 min. Then, after 2 hours, they were placed into context B for extinction training. Mice were first presented with four trials of the CS^- followed by 12 trials of the CS^+. On day 2, they received an additional two extinction training sessions in context B separated by 6 hours during which they experienced 24 CS^+ trials. On day 3, mice were tested for extinction memory in context B with four CS^+ presentations. Two hours later, mice were tested for context-dependent fear renewal by placing them back into context A and presenting four trials of the CS^+. ANY-maze (Stoelting) was used to automatically detect freezing behavior and to track body center position within the arena at 30 frames per second. Between behavioral sessions, mice remained in their home cages within a sound-attenuating chamber.

TRAP protocol

Two weeks following surgical infusion of AAV2/9-hSyn1-DIO-TVA950-2A-EGFP-2A-oG into the vH, mice underwent fear and extinction training over 2 days as described above. On day 3, they were transported to the testing room and left in their home cages in a sound-attenuating chamber for 3 hours. They were then either placed into the extinction context B for 20 min or remained in their home cage. Both context-exposed and home-caged mice were administered 4-OHT (50 mg/kg ip) at the end of the 20 min. They were then left in their home cage in the sound-attenuating chamber for a further 3 hours before returning to the colony room. Eight days later, mice underwent a second surgery during which EnvA-N2C-RVdG-tdTomato was infused into the vH. After 6 days, they were perfused, and their brains were harvested.

Optogenetics

Optic fibers (200 μm core, 0.37 NA; Thorlabs) were cleaved to the appropriate length and secured to ceramic ferrules (1.25 mm in diameter, 230-μm bore, Senko). After surgical implantation at behavioral testing, ceramic mating sleeves (Senko) connected optic fibers to optic patch cables (0.37 NA; Doric Lenses), which were, in turn, connected to an optical rotary joint (Doric Lenses). For bilateral light delivery, patch cables were first connected to light splitter (Doric Lenses). The commutator was attached to an additional patch cable (0.37 NA; Doric Lenses) that directly fed to a diode-pumped solid-state laser, emitting green light (561 nm; Cobolt). Laser light delivery was controlled via an ANY-maze Transistor-Transistor-Logic (TTL) output signal to a custom-built digital input/output interface that triggered the laser. Laser light was applied continuously at a power intensity of 10 mW measured

from the optic fiber tip during the CS period at extinction training sessions. For optogenetic behavioral experiments without electrophysiological recordings, light was delivered at Ext 1 trials 5 to 12, Ext 2 trials 3 to 24, and Ext 3 trials 3 to 24. For optogenetic behavioral experiments with electrophysiological recordings, light was delivered at Ext 1 trials 5 to 12, Ext 2 trials 1 to 24, and Ext 3 trials 1 to 24.

Behavior with electrophysiological recordings

Ten days following surgery, mice were familiarized to the testing room and handling procedures, which included cable tethering to the recording system. The next day, tetrodes were lowered roughly 200 μm while monitoring electrophysiological hallmarks of the stratum pyramidale (i.e., sharp wave ripples and theta oscillations) and multiunit spiking. Twenty-four hours later, mice underwent fear and extinction behavioral testing as outlined above. In between each behavioral session, neuronal activity during sleep/rest was recorded in the home cage 30 min before the start and 30 min after the end of the session. Electrophysiological signals were aligned to behavior via TTL outputs sent from ANY-maze to the recording system for cue presentation, electrical shock delivery, laser delivery, and individual camera frames.

Drugs

4-OHT (Sigma-Aldrich, H6278) was dissolved in anhydrous ethanol at a concentration of 20 mg/ml by shaking incubation at 37°C for 10 min. A 1:4 mixture of castor oil/sunflower seed oil (Sigma-Aldrich, 259853 and S5007) was then added, and the ethanol was evaporated by vacuum centrifugation. The final concentration of the 4-OHT solution was 10 mg/ml and was administered the same day at a dose of 50 mg/kg ip and at a volume of 5 ml/kg.

Histology

Mice were overdosed with a ketamine/xylazine cocktail and transcardially perfused with phosphate-buffered saline (PBS; pH 7.4) followed by 4% formaldehyde. Brains were extracted and postfixed overnight in 4% formaldehyde at 4°C. Brains were sectioned coronally at a thickness of 50 μm using a vibratome (Leica Microsystems, VT1000 S). For electrophysiology experiments, before perfusion, mice were anesthetized with isoflurane, and tetrode positions were marked by electrolytic lesions. After sections were prepared, the tip of each tetrode was located, and only tetrodes positioned in the vH were included for analysis.

Immunohistochemistry

Free-floating brain sections were blocked with 5% normal donkey serum in 0.1% Triton X-100 in PBS (PBS-T) at room temperature for 2 hours. Sections were then incubated for 72 hours at 4°C with PBS-T containing a combination of the following primary antibodies: chicken polyclonal anti-GFP (1:1000; Abcam, ab13970), rabbit polyclonal anti-GFP (1:1000; Abcam, ab6556), and goat polyclonal anti-tdTomato (1:1000; SICGEN, AB8181). Primary antibody incubation was followed by incubation for 2 hours at room temperature with PBS-T containing a combination of the following secondary antibodies: donkey anti-chicken Alexa Fluor 488 (1:1000; Jackson ImmunoResearch Laboratories, 703545145), donkey anti-rabbit Alexa Fluor 488 (1:1000; Invitrogen, A32790), and donkey anti-goat Alexa Fluor 555 (1:1000; Invitrogen, A32816). Between incubations, sections were washed in PBS-T three times for 5 min. After mounting onto slides, sections were incubated in 4′,6-diamidino-2-phenylindole (DAPI) solution (Sigma-Aldrich, MBD0015) to label cell nuclei, then coverslipped with aqueous mounting medium (Aqua-Poly/Mount, Polysciences), and stored at 4°C.

Microscopy and cell quantification

For TRAP experiments, every sixth section between bregma 3.1 and −5.8 mm was immunostained for GFP and tdTomato. Sections containing the vH (bregma: −2.8 to −3.8 mm) were imaged on a confocal laser scanning microscope (Zeiss, LSM 880) with a 20× objective. The remaining sections were imaged on a slide scanning microscope (3dHistech, Pannoramic 250 Flash II). Neurons positive for GFP and/or tdTomato were manually counted in ImageJ using the cell counter plugin. Cell density was calculated as: number of neurons/area in which neurons were counted. The percentage of total input neurons was calculated as: (number of regional $tdTomato^+$ neurons/total $tdTomato^+$ neurons) × 100.

Spike detection and unit classification

Extracellular electrophysiological signals were acquired using an Intan RHD2000 Evaluation Board at a sampling rate of 20 kHz. Neuronal spikes were detected offline by digitally filtering the signal (0.5 to 5 kHz) and detecting events 5 SD above the root mean squared signal in 0.2-ms sliding windows. For each spike waveform, 32 data points were collected in a 1.6-ms window. Principal components analysis was performed on spike waveforms to extract the first three components for each tetrode channel. These spike features were automatically sorted into individual units using KlustaKwik (http://klustakwik.sourceforge.net/) followed by manual curation in Klusters (http://neurosuite.sourceforge.net/). Well-isolated single units were verified by their waveform shape, waveform amplitude modulation across tetrode channels, presence of a refractory period in the autocorrelogram, and cross-correlogram with other units to assess for a common refractory period and excitatory/inhibitory interactions and stability of spike features over time.

Neuronal data analysis

Putative interneuron classification

Putative pyramidal neurons and interneurons were distinguished by first clustering (K-means, $K = 2$) averaged spike waveforms to produce two clusters with spike properties characteristic of each class. Units with narrow spike half-width and a short trough-to-peak latency along with a mean firing rate of >8 Hz across the experiment were classified as putative interneurons.

Local field potentials

The 20-kHz signal of each channel was down-sampled to 1250 Hz. Analysis of phase locking to theta oscillations was performed using the MATLAB toolbox for circular statistics (www.mathworks.com/matlabcentral/fileexchange/10676-circular-statistics-toolbox-directional-statistics). The local field potential (LFP) of each channel was theta filtered (4 to 12 Hz, Butterworth third order), and the instantaneous phase was determined with the Hilbert transform. The instantaneous phase for each channel of a given tetrode were averaged in time (circular mean), and the spikes of each unit were assigned a phase angle using the signal from the tetrode on which the unit was recorded. Units with significant phase locking were determined with Rayleigh's test for circular uniformity ($P < 0.05$). For significantly phase-locked neurons that fired a minimum of 50 spikes during the epoch examined, we calculated the strength of their phase locking as the mean resultant vector

length of the spike phase angles. To construct time-frequency spectrograms, a continuous wavelet transform (Morlet wavelet, 32 voices per octave) was applied to the LFP signals during a given CS^+ trial for each channel. The power was calculated and averaged across all channels, trials, and mice. For power spectral density estimates, Welch′s method was applied to LFP signals during a given epoch for each channel (Hamming window, 3-s segments, 75% overlap) and then averaged across channels. To compare changes in power pre- and post-CS onset, power at each frequency was normalized by dividing by the total power during the pre-CS period (relative power).

Sleep state

For sleep/rest sessions, NREM and REM episodes were identified using LFP and EMG signals. LFP activity in each tetrode was filtered (third order Butterworth) for theta (4 to 12 Hz) and delta (1 to 4 Hz) and then Hilbert transformed to extract their instantaneous amplitudes (smoothed with Gaussian kernel, σ = 1 s). The ratio of theta:delta amplitude was taken and averaged across tetrodes, and *z* score was normalized. Periods with a relatively high theta:delta ratio (peak ratio of >1.5 SD and falling to 0.5 SD) were identified as candidate REM episodes, while all other time points were considered candidate NREM episodes. EMG signals were band-pass–filtered (100 to 1000 Hz, third order Butterworth), rectified, and low-pass filtered (20 Hz, Butterworth third order) to create a linear envelope. After down-sampling to 1250 Hz, the signal was normalized between 0 and 1. Time points in the EMG signal where the normalized amplitude rose above a set threshold (set at 0.08) were considered as waking periods. These wake periods were excluded from candidate NREM and REM events, and only episodes lasting a minimum of 10 s were included for further analysis.

Cue response

Firing rate across each session was obtained in 1-ms bins and then smoothed by convolution with a Gaussian kernel (σ = 200 ms). Firing rate was extracted for each CS^+ trial at extinction test beginning at 30 s preceding CS onset to 30 s following CS onset. CS^+ trials were averaged then binned into 200-ms nonoverlapping windows. To identify units that were significantly CS responsive, a permutation test was performed for each unit. The Student′s *t* statistic was calculated with pre-CS and CS time points taken as independent samples. This value was compared to a surrogate distribution created by shuffling the actual trial-averaged firing rate series and recalculating the *t* statistic over 1000 repetitions. Units whose observed statistic fell at the extremes of the surrogate distribution ($P < 0.001$) were considered responsive, with a positive value indicating activation and a negative value indicating inhibition.

Spatial firing

Only time points with an instantaneous velocity greater than 2 cm/s measured from the body′s center point were included for analysis. Each spike was assigned to a 1-by-1 cm^2 maze bin, which we refer to as a pixel. Firing rate was calculated by dividing the number of spikes occurring in each bin with the occupancy time in that bin. This raw map was then smoothed with a Gaussian kernel (σ = 3 cm) in the *x* and *y* direction. For visualization purposes only, two-dimensional (2D) maps were linearized by averaging pixels located at the same distance from the centermost maze point. Active pixels were defined as spatial bins with a firing rate exceeding 20% of the peak rate in any spatial bin. Spatial information in bits per spike was calculated with the following formula (*92*)

$$\text{Information content} = \sum_{i=1}^{N} p_i \left(\frac{F_i}{F}\right) \log_2\left(\frac{F_i}{F}\right)$$

where for spatial bins, $i = 1, \ldots, N$; p_i is the probability of occupying bin *i*; F_i is the firing rate at bin *i*; and *F* is the overall mean firing rate.

Zone response

Smoothed spatial firing rate maps were obtained for all units and sessions, and the 2D maps were unwrapped to create a matrix with dimensions equal to the number of maze pixels (676 for a 26-by-26 cm^2 maze divided into a grid of 1-cm bins). Principal components analysis was applied to this matrix, and the first eigenvector was visualized to confirm high variance in the center pixels (fig. S4F). The correlation between each unit′s spatial firing map and eigenvector 1 was calculated as the cosine similarity between the two vectors. Units with a correlation of >0.3 were categorized as center-activated, while units with a correlation of < −0.3 were categorized as periphery-activated. Only units from mice that explored more than 30% of both the center and periphery zones were included in analyses. To examine activity and behavior in each zone, we defined the center zone as a square area located 8 cm from the maze walls, while the periphery zone was set to the remaining bordering area.

Speed modulation

Instantaneous speed was interpolated to 200-ms intervals. For each unit, the Pearson′s *r* correlation was taken between the animal′s speed and unit′s firing rate (200-ms bins) throughout the 10-min acclimation period at the extinction test. A unit was considered to be significantly speed-modulated if $P < 0.05$. The speed in each zone was determined by extracting time stamps at which a given mouse occupied the center or periphery zones.

Reactivation

To quantify the similarity of neuronal activity patterns during behavior and sleep, we calculated the explained variance as described previously (*50*). First, spike trains in 100-ms bins were extracted during the CS period of each trial for behavioral sessions or during NREM and REM episodes for sleep sessions. Pairwise correlations in the spike trains of each pair of units were calculated with Pearson′s *r* using the same neurons for every session. A set of correlation coefficients was obtained for each behavioral session (CS period), presleep session (NREM or REM), and postsleep session (NREM or REM). The Pearson′s *r* correlation between the coefficients of each pair of sessions was then calculated and used to compute the explained variance (EV) of postsleep activity by CS activity after controlling for presleep activity

$$\text{EV}_{\text{CS,Post|Pre}} = \left[\frac{r_{\text{CS,Post}} - r_{\text{CS,Pre}} \times r_{\text{Post,Pre}}}{\sqrt{(1 - r^2_{\text{CS,Pre}})(1 - r^2_{\text{Post,Pre}})}}\right]^2$$

where $r_{\text{CS,Post}}$ and $r_{\text{CS,Pre}}$ are the correlation coefficients between the set of pairwise correlations obtained during CS trials with the set obtained at post- and presleep, respectively. The term $r_{\text{Post,Pre}}$ refers to the correlation between the pairwise coefficients for post- and presleep. As a control measure, we also calculated the explained variance of presleep activity by CS activity after controlling for postsleep activity ($\text{EV}_{\text{CS,Pre|Post}}$).

Zone decoding

Time stamps of trajectories from the periphery zone into the center zone (minimum of 1 s and equal samples in each zone) were extracted for each mouse from the extinction test exploration period. The corresponding firing rate (100-ms bins) of all pyramidal neurons in individual mice was selected, and each time bin was labeled according to occupation of the periphery or center zones. The data were then randomly split (50/50) into training and holdout test samples with a balanced number of labels. Only mice with a total of at least 3 s in each zone were included for analysis. Training samples were used to train a binary linear classifier (Support Vector Machine, MATLAB Classification Learner application) with cross-validation (10-fold) and then applied to test samples with accuracy evaluated as the percentage of correctly labeled samples. This process was repeated 20 times per mouse, and values were averaged across mice in the $EYFP^{BLA\rightarrow vH}$ and $Arch^{BLA\rightarrow vH}$ groups for each iteration. The mean and SD of the accuracy across iterations was calculated, and significance of this sampling distribution was tested using a z test.

Position decoding

Using the first 85% of data acquired at the extinction test session, we generated spatial firing rate maps as described above ("Spatial firing" section in Materials and Methods). With the remaining 15% of the session, we extracted the position of the mouse in the maze (1-by-1 cm bins) and the spike counts of pyramidal neurons in 1-s time intervals. The probability of occupying each position was then predicted for individual mice using the following equation (*41*)

$$P(x|s) = CP(x)\left[\prod_{i=1}^{N} f_i(x)^{s_i}\right]\exp\left[-\tau\sum_{i=1}^{N} f_i(x)\right]$$

where $f_i(x)$ is the spatial firing map of neuron i; s is the population spike vector at time t; τ is the time interval; $P(x)$ is the spatial prior, which was a 2D Gaussian continuity constraint centered on the position predicted at t-1 and with an SD equal to the speed (centimeter per second) at t; and C is a normalization factor to guarantee that $\sum_x P(x|s) = 1$. The position with the highest probability was taken as the predicted position at time t.

Statistical analysis

Analyses were performed using custom scripts written in MATLAB (MathWorks). Statistics were performed using R and GraphPad Prism. All datasets were tested for normality using the Kolmogorov-Smirnov test, and if found to be not normally distributed, then nonparametric tests were applied. All null hypothesis tests were two-tailed. Analyses of variance (ANOVAs) were followed by post hoc tests if a main effect or interaction was observed. In the case of multiple comparisons, significance was evaluated with Sidak and Tukey's post hoc tests or the two-stage step-up method of Benjamini, Krieger, and Yekutieli with a false discovery rate (FDR) of 5%. Box and whisker plots show median, interquartile range (25th and 75th percentiles), and outlier values while bar graphs show means ± SEM unless specified otherwise. Asterisks in the figures represent P values corresponding to the following thresholds: $^{*}P < 0.05$; $^{**}P < 0.01$; $^{***}P < 0.001$.

Supplementary Materials

This PDF file includes:

Figs. S1 to S5

View/request a protocol for this paper from *Bio-protocol*.

REFERENCES AND NOTES

1. S. Trask, E. A. Thrailkill, M. E. Bouton, Occasion setting, inhibition, and the contextual control of extinction in Pavlovian and instrumental (operant) learning. *Behav. Processes* **137**, 64–72 (2017).
2. M. E. Bouton, Context and behavioral processes in extinction. *Learn. Mem.* **11**, 485–494 (2004).
3. S. Maren, K. L. Phan, I. Liberzon, The contextual brain: Implications for fear conditioning, extinction and psychopathology. *Nat. Rev. Neurosci.* **14**, 417–428 (2013).
4. N. C. Tronson, K. A. Corcoran, V. Jovasevic, J. Radulovic, Fear conditioning and extinction: Emotional states encoded by distinct signaling pathways. *Trends Neurosci.* **35**, 145–155 (2012).
5. R. L. Clem, D. Schiller, New learning and unlearning strangers or accomplices in threat memory attenuation? *Trends Neurosci.* **39**, 340–351 (2016).
6. M. E. Bouton, D. A. King, Contextual control of the extinction of conditioned fear-tests for the associative value of the context. *J. Exp. Psychol.* **9**, 248–265 (1983).
7. J. J. Kim, R. A. Rison, M. S. Fanselow, Effects of amygdala, hippocampus, and periaqueductal gray lesions on short- and long-term contextual fear. *Behav. Neurosci.* **107**, 1093–1098 (1993).
8. W. A. Falls, M. J. Miserendino, M. Davis, Extinction of fear-potentiated startle: Blockade by infusion of an NMDA antagonist into the amygdala. *J. Neurosci.* **12**, 854–863 (1992).
9. P. Tovote, J. P. Fadok, A. Luthi, Neuronal circuits for fear and anxiety. *Nat. Rev. Neurosci.* **16**, 317–331 (2015).
10. C. Herry, S. Ciocchi, V. Senn, L. Demmou, C. Müller, A. Lüthi, Switching on and off fear by distinct neuronal circuits. *Nature* **454**, 600–606 (2008).
11. E. Likhtik, D. Popa, J. Apergis-Schoute, G. A. Fidacaro, D. Paré, Amygdala intercalated neurons are required for expression of fear extinction. *Nature* **454**, 642–645 (2008).
12. N. Whittle, J. Fadok, K. P. MacPherson, R. Nguyen, P. Botta, S. B. E. Wolff, C. Müller, C. Herry, P. Tovote, A. Holmes, N. Singewald, A. Lüthi, S. Ciocchi, Central amygdala micro-circuits mediate fear extinction. *Nat. Commun.* **12**, 4156 (2021).
13. K. M. Hagihara, O. Bukalo, M. Zeller, A. Aksoy-Aksel, N. Karalis, A. Limoges, T. Rigg, T. Campbell, A. Mendez, C. Weinholtz, M. Mahn, L. S. Zweifel, R. D. Palmiter, I. Ehrlich, A. Lüthi, A. Holmes, Intercalated amygdala clusters orchestrate a switch in fear state. *Nature* **594**, 403–407 (2021).
14. X. Y. Zhang, J. Kim, S. Tonegawa, Amygdala reward neurons form and store fear extinction memory. *Neuron* **105**, 1077–1093.e7 (2020).
15. V. Laurent, R. F. Westbrook, Inactivation of the infralimbic but not the prelimbic cortex impairs consolidation and retrieval of fear extinction. *Learn. Mem.* **16**, 520–529 (2009).
16. F. H. Do-Monte, G. Manzano-Nieves, K. Quiñones-Laracuente, L. Ramos-Medina, G. J. Quirk, Revisiting the role of infralimbic cortex in fear extinction with optogenetics. *J. Neurosci.* **35**, 3607–3615 (2015).
17. O. Bukalo, C. R. Pinard, S. Silverstein, C. Brehm, N. D. Hartley, N. Whittle, G. Colacicco, E. Busch, S. Patel, N. Singewald, A. Holmes, Prefrontal inputs to the amygdala instruct fear extinction memory formation. *Sci. Adv.* **1**, e1500251 (2015).
18. C. Dejean, J. Courtin, N. Karalis, F. Chaudun, H. Wurtz, T. C. M. Bienvenu, C. Herry, Prefrontal neuronal assemblies temporally control fear behaviour. *Nature* **535**, 420–424 (2016).
19. B. A. Silva, S. Astori, A. M. Burns, H. Heiser, L. van den Heuvel, G. Santoni, M. F. Martinez-Reza, C. Sandi, J. Gräff, A thalamo-amygdalar circuit underlying the extinction of remote fear memories. *Nat. Neurosci.* **24**, 964–974 (2021).
20. N. S. Canteras, L. W. Swanson, Projections of the ventral subiculum to the amygdala, septum, and hypothalamus: A Phal anterograde tract-tracing study in the rat. *J. Comp. Neurol.* **324**, 180–194 (1992).
21. A. Pitkanen, M. Pikkarainen, N. Nurminen, A. Ylinen, Reciprocal connections between the amygdala and the hippocampal formation, perirhinal cortex, and postrhinal cortex in rat: A review. *Ann. N. Y. Acad. Sci.* **911**, 369–391 (2000).
22. L. A. Cenquizca, L. W. Swanson, Spatial organization of direct hippocampal field CA1 axonal projections to the rest of the cerebral cortex. *Brain Res. Rev.* **56**, 1–26 (2007).
23. M. S. Fanselow, H. W. Dong, Are the dorsal and ventral hippocampus functionally distinct structures? *Neuron* **65**, 7–19 (2010).
24. S. Ciocchi, J. Passecker, H. Malagon-Vina, N. Mikus, T. Klausberger, Selective information routing by ventral hippocampal CA1 projection neurons. *Science* **348**, 560–563 (2015).

25. S. Royer, A. Sirota, J. Patel, G. Buzsáki, Distinct representations and theta dynamics in dorsal and ventral hippocampus. *J. Neurosci.* **30**, 1777–1787 (2010).
26. R. W. Komorowski, C. G. Garcia, A. Wilson, S. Hattori, M. W. Howard, H. Eichenbaum, Ventral hippocampal neurons are shaped by experience to represent behaviorally relevant contexts. *J. Neurosci.* **33**, 8079–8087 (2013).
27. C. Xu, S. Krabbe, J. Gründemann, P. Botta, J. P. Fadok, F. Osakada, D. Saur, B. F. Grewe, M. J. Schnitzer, E. M. Callaway, A. Lüthi, Distinct hippocampal pathways mediate dissociable roles of context in memory retrieval. *Cell* **167**, 961–972.e16 (2016).
28. J. C. Jimenez, K. Su, A. R. Goldberg, V. M. Luna, J. S. Biane, G. Ordek, P. Zhou, S. K. Ong, M. A. Wright, L. Zweifel, L. Paninski, R. Hen, M. A. Kheirbek, Anxiety cells in a hippocampal-hypothalamic circuit. *Neuron* **97**, 670–683.e6 (2018).
29. T. Forro, E. Volitaki, H. Malagon-Vina, T. Klausberger, T. Nevian, S. Ciocchi, Anxiety-related activity of ventral hippocampal interneurons. *Prog. Neurobiol.* **219**, 102368 (2022).
30. J. C. Jimenez, J. E. Berry, S. C. Lim, S. K. Ong, M. A. Kheirbek, R. Hen, Contextual fear memory retrieval by correlated ensembles of ventral CA1 neurons. *Nat. Commun.* **11**, 3492 (2020).
31. T. A. LeGates, M. D. Kvarta, J. R. Tooley, T. C. Francis, M. K. Lobo, M. C. Creed, S. M. Thompson, Reward behaviour is regulated by the strength of hippocampus–nucleus accumbens synapses. *Nature* **564**, 258–262 (2018).
32. J. A. Hobin, J. Ji, S. Maren, Ventral hippocampal muscimol disrupts context-specific fear memory retrieval after extinction in rats. *Hippocampus* **16**, 174–182 (2006).
33. R. Marek, J. Jin, T. D. Goode, T. F. Giustino, Q. Wang, G. M. Acca, R. Holehonnur, J. E. Ploski, P. J. Fitzgerald, T. Lynagh, J. W. Lynch, S. Maren, P. Sah, Author correction: Hippocampus-driven feed-forward inhibition of the prefrontal cortex mediates relapse of extinguished fear. *Nat. Neurosci.* **21**, 1291–1291 (2018).
34. J. Ji, S. Maren, Hippocampal involvement in contextual modulation of fear extinction. *Hippocampus* **17**, 749–758 (2007).
35. D. Sierra-Mercado, N. Padilla-Coreano, G. J. Quirk, Dissociable roles of prelimbic and infralimbic cortices, ventral hippocampus, and basolateral amygdala in the expression and extinction of conditioned fear. *Neuropsychopharmacology* **36**, 529–538 (2011).
36. B. Zhang, C. Y. Li, X. S. Wang, The effect of hippocampal NMDA receptor blockade by MK-801 on cued fear extinction. *Behav. Brain Res.* **332**, 200–203 (2017).
37. A. C. Felix-Ortiz, A. Beyeler, C. Seo, C. A. Leppla, C. P. Wildes, K. M. Tye, BLA to vHPC inputs modulate anxiety-related behaviors. *Neuron* **79**, 658–664 (2013).
38. G. Pi, D. Gao, D. Wu, Y. Wang, H. Lei, W. Zeng, Y. Gao, H. Yu, R. Xiong, T. Jiang, S. Li, X. Wang, J. Guo, S. Zhang, T. Yin, T. He, D. Ke, R. Li, H. Li, G. Liu, X. Yang, M.-H. Luo, X. Zhang, Y. Yang, J.-Z. Wang, Posterior basolateral amygdala to ventral hippocampal CA1 drives approach behaviour to exert an anxiolytic effect. *Nat. Commun.* **11**, 183 (2020).
39. A. Beyeler, P. Namburi, G. F. Glober, C. Simonnet, G. G. Calhoon, G. F. Conyers, R. Luck, C. P. Wildes, K. M. Tye, Divergent routing of positive and negative information from the amygdala during memory retrieval. *Neuron* **90**, 348–361 (2016).
40. W. E. Allen, L. A. DeNardo, M. Z. Chen, C. D. Liu, K. M. Loh, L. E. Fenno, C. Ramakrishnan, K. Deisseroth, L. Luo, Thirst-associated preoptic neurons encode an aversive motivational drive. *Science* **357**, 1149–1155 (2017).
41. I. R. Wickersham, D. C. Lyon, R. J. O. Barnard, T. Mori, S. Finke, K.-K. Conzelmann, J. A. T. Young, E. M. Callaway, Monosynaptic restriction of transsynaptic tracing from single, genetically targeted neurons. *Neuron* **53**, 639–647 (2007).
42. L. A. DeNardo, C. D. Liu, W. E. Allen, E. L. Adams, D. Friedmann, L. Fu, C. J. Guenthner, M. Tessier-Lavigne, L. Luo, Temporal evolution of cortical ensembles promoting remote memory retrieval. *Nat. Neurosci.* **22**, 460–469 (2019).
43. P. H. Janak, K. M. Tye, From circuits to behaviour in the amygdala. *Nature* **517**, 284–292 (2015).
44. M. A. Penzo, C. Gao, The paraventricular nucleus of the thalamus: An integrative node underlying homeostatic behavior. *Trends Neurosci.* **44**, 538–549 (2021).
45. J. Jackson, J. B. Smith, A. K. Lee, The anatomy and physiology of claustrum-cortex interactions. *Annu. Rev. Neurosci.* **43**, 231–247 (2020).
46. M. J. Dolleman-van der Weel, A. L. Griffin, H. T. Ito, M. L. Shapiro, M. P. Witter, R. P. Vertes, T. A. Allen, The nucleus reuniens of the thalamus sits at the nexus of a hippocampus and medial prefrontal cortex circuit enabling memory and behavior. *Learn. Mem.* **26**, 191–205 (2019).
47. P. C. Holland, M. E. Bouton, Hippocampus and context in classical conditioning. *Curr. Opin. Neurobiol.* **9**, 195–202 (1999).
48. M. A. Wilson, B. L. McNaughton, Reactivation of hippocampal ensemble memories during sleep. *Science* **265**, 676–679 (1994).
49. J. G. Klinzing, N. Niethard, J. Born, Publisher correction: Mechanisms of systems memory consolidation during sleep. *Nat. Neurosci.* **22**, 1743–1744 (2019).
50. H. S. Kudrimoti, C. A. Barnes, B. L. McNaughton, Reactivation of hippocampal cell assemblies: Effects of behavioral state, experience, and EEG dynamics. *J. Neurosci.* **19**, 4090–4101 (1999).
51. J. Lesting, R. T. Narayanan, C. Kluge, S. Sangha, T. Seidenbecher, H. C. Pape, Patterns of coupled theta activity in amygdala-hippocampal-prefrontal cortical circuits during fear extinction. *PLOS ONE* **6**, e21714 (2011).
52. E. Likhtik, J. M. Stujenske, M. A. Topiwala, A. Z. Harris, J. A. Gordon, Prefrontal entrainment of amygdala activity signals safety in learned fear and innate anxiety. *Nat. Neurosci.* **17**, 106–113 (2014).
53. G. Buzsaki, Theta oscillations in the hippocampus. *Neuron* **33**, 325–340 (2002).
54. K. B. Kjelstrup, T. Solstad, V. H. Brun, T. Hafting, S. Leutgeb, M. P. Witter, E. I. Moser, M.-B. Moser, Finite scale of spatial representation in the hippocampus. *Science* **321**, 140–143 (2008).
55. A. T. Keinath, M. E. Wang, E. G. Wann, R. K. Yuan, J. T. Dudman, I. A. Muzzio, Precise spatial coding is preserved along the longitudinal hippocampal axis. *Hippocampus* **24**, 1533–1548 (2014).
56. K. Zhang, I. Ginzburg, B. L. McNaughton, T. J. Sejnowski, Interpreting neuronal population activity by reconstruction: Unified framework with application to hippocampal place cells. *J. Neurophysiol.* **79**, 1017–1044 (1998).
57. M. A. A. van der Meer, A. A. Carey, Y. Tanaka, Optimizing for generalization in the decoding of internally generated activity in the hippocampus. *Hippocampus* **27**, 580–595 (2017).
58. M. E. Bouton, Context, time, and memory retrieval in the interference paradigms of Pavlovian learning. *Psychol. Bull.* **114**, 80–99 (1993).
59. F. Gore, E. C. Schwartz, B. C. Brangers, S. Aladi, J. M. Stujenske, E. Likhtik, M. J. Russo, J. A. Gordon, C. D. Salzman, R. Axel, Neural representations of unconditioned stimuli in basolateral amygdala mediate innate and learned responses. *Cell* **162**, 134–145 (2015).
60. P. Namburi, A. Beyeler, S. Yorozu, G. G. Calhoon, S. A. Halbert, R. Wichmann, S. S. Holden, K. L. Mertens, M. Anahtar, A. C. Felix-Ortiz, I. R. Wickersham, J. M. Gray, K. M. Tye, A circuit mechanism for differentiating positive and negative associations. *Nature* **520**, 675–678 (2015).
61. J. Gründemann, Y. Bitterman, T. Lu, S. Krabbe, B. F. Grewe, M. J. Schnitzer, A. Lüthi, Amygdala ensembles encode behavioral states. *Science* **364**, 254–262 (2019).
62. P. Kyriazi, D. B. Headley, D. Pare, Multi-dimensional coding by basolateral amygdala neurons. *Neuron* **99**, 1315–1328.e5 (2018).
63. X. Zhang, B. Li, Population coding of valence in the basolateral amygdala. *Nat. Commun.* **9**, 5195 (2018).
64. M. Sol Fustinana, M. S. Fustiñana, T. Eichlisberger, T. Bouwmeester, Y. Bitterman, A. Lüthi, State-dependent encoding of exploratory behaviour in the amygdala. *Nature* **592**, 267–271 (2021).
65. J. Courtin, Y. Bitterman, S. Müller, J. Hinz, K. M. Hagihara, C. Müller, A. Lüthi, A neuronal mechanism for motivational control of behavior. *Science* **375**, 1–13 (2022).
66. J. Felsenberg, P. F. Jacob, T. Walker, O. Barnstedt, A. J. Edmondson-Stait, M. W. Pleijzier, N. Otto, P. Schlegel, N. Sharifi, E. Perisse, C. S. Smith, J. S. Lauritzen, M. Costa, G. S. X. E. Jefferis, D. D. Bock, S. Waddell, Integration of parallel opposing memories underlies memory extinction. *Cell* **175**, 709–722.e15 (2018).
67. R. Kalisch, A. M. V. Gerlicher, S. Duvarci, A dopaminergic basis for fear extinction. *Trends Cogn. Sci.* **23**, 274–277 (2019).
68. L. X. Cai, K. Pizano, G. W. Gundersen, C. L. Hayes, W. T. Fleming, S. Holt, J. M. Cox, I. B. Witten, Distinct signals in medial and lateral VTA dopamine neurons modulate fear extinction at different times. *eLife* **9**, e54936 (2020).
69. R. Luo, A. Uematsu, A. Weitemier, L. Aquili, J. Koivumaa, T. J. Mc Hugh, J. P. Johansen, A dopaminergic switch for fear to safety transitions. *Nat. Commun.* **9**, 2483 (2018).
70. B. F. Grewe, J. Gründemann, L. J. Kitch, J. A. Lecoq, J. G. Parker, J. D. Marshall, M. C. Larkin, P. E. Jercog, F. Grenier, J. Z. Li, A. Lüthi, M. J. Schnitzer, Neural ensemble dynamics underlying a long-term associative memory. *Nature* **543**, 670–675 (2017).
71. G. Buzsaki, E. I. Moser, Memory, navigation and theta rhythm in the hippocampal-entorhinal system. *Nat. Neurosci.* **16**, 130–138 (2013).
72. N. Padilla-Coreano, S. Canetta, R. M. Mikofsky, E. Alway, J. Passecker, M. V. Myroshnychenko, A. L. Garcia-Garcia, R. Warren, E. Teboul, D. R. Blackman, M. P. Morton, S. Hupalo, K. M. Tye, C. Kellendonk, D. A. Kupferschmidt, J. A. Gordon, Hippocampal-prefrontal theta transmission regulates avoidance behavior. *Neuron* **104**, 601–610.e4 (2019).
73. J. A. Cardin, M. Carlén, K. Meletis, U. Knoblich, F. Zhang, K. Deisseroth, L. H. Tsai, C. I. Moore, Targeted optogenetic stimulation and recording of neurons in vivo using cell-type-specific expression of Channelrhodopsin-2. *Nat. Protoc.* **5**, 247–254 (2010).
74. S. Mikulovic, S. Pupe, H. M. Peixoto, G. C. do Nascimento, K. Kullander, A. B. L. Tort, R. N. Leão, On the photovoltaic effect in local field potential recordings. *Neurophotonics* **3**, 015002 (2016).
75. K. Kim, M. Vöröslakos, J. P. Seymour, K. D. Wise, G. Buzsáki, E. Yoon, Artifact-free and high-temporal-resolution in vivo opto-electrophysiology with microLED optoelectrodes. *Nat. Commun.* **11**, 2063 (2020).
76. H. Hintiryan, I. Bowman, D. L. Johnson, L. Korobkova, M. Zhu, N. Khanjani, L. Gou, L. Gao, S. Yamashita, M. S. Bienkowski, L. Garcia, N. N. Foster, N. L. Benavidez, M. Y. Song, D. Lo, K. R.

Cotter, M. Becerra, S. Aquino, C. Cao, R. P. Cabeen, J. Stanis, M. Fayzullina, S. A. Ustrell, T. Boesen, A. J. Tugangui, Z. G. Zhang, B. Peng, M. S. Fanselow, P. Golshani, J. D. Hahn, I. R. Wickersham, G. A. Ascoli, L. I. Zhang, H. W. Dong, Connectivity characterization of the mouse basolateral amygdalar complex. *Nat. Commun.* **12**, 2859 (2021).

77. L. R. Bevilaqua, J. S. Bonini, J. I. Rossato, L. A. Izquierdo, M. Cammarota, I. Izquierdo, The entorhinal cortex plays a role in extinction. *Neurobiol. Learn. Mem.* **85**, 192–197 (2006).
78. E. Baldi, C. Bucherelli, Entorhinal cortex contribution to contextual fear conditioning extinction and reconsolidation in rats. *Neurobiol. Learn. Mem.* **110**, 64–71 (2014).
79. J. Ji, S. Maren, Lesions of the entorhinal cortex or fornix disrupt the context-dependence of fear extinction in rats. *Behav. Brain Res.* **194**, 201–206 (2008).
80. A. P. Yonelinas, C. Ranganath, A. D. Ekstrom, B. J. Wiltgen, A contextual binding theory of episodic memory: Systems consolidation reconsidered. *Nat. Rev. Neurosci.* **20**, 364–375 (2019).
81. A. Bechara, D. Tranel, H. Damasio, R. Adolphs, C. Rockland, A. R. Damasio, Double dissociation of conditioning and declarative knowledge relative to the amygdala and hippocampus in humans. *Science* **269**, 1115–1118 (1995).
82. D. C. Knight, N. S. Waters, P. A. Bandettini, Neural substrates of explicit and implicit fear memory. *Neuroimage* **45**, 208–214 (2009).
83. M. S. Bienkowski, I. Bowman, M. Y. Song, L. Gou, T. Ard, K. Cotter, M. Zhu, N. L. Benavidez, S. Yamashita, J. Abu-Jaber, S. Azam, D. Lo, N. N. Foster, H. Hintiryan, H. W. Dong, Integration of gene expression and brain-wide connectivity reveals the multiscale organization of mouse hippocampal networks. *Nat. Neurosci.* **21**, 1628–1643 (2018).
84. R. W. S. Wee, A. F. MacAskill, Biased connectivity of brain-wide inputs to ventral subiculum output neurons. *Cell Rep.* **30**, 3644–3654.e6 (2020).
85. M. M. Gergues, K. J. Han, H. S. Choi, B. Brown, K. J. Clausing, V. S. Turner, I. D. Vainchtein, A. V. Molofsky, M. A. Kheirbek, Circuit and molecular architecture of a ventral hippocampal network. *Nat. Neurosci.* **24**, 1444–1452 (2021).
86. R. AlSubaie, R. W. Wee, A. Ritoux, K. Mishchanchuk, J. Passlack, D. Regester, A. F. MacAskill, Control of parallel hippocampal output pathways by amygdalar long-range inhibition. *eLife* **10**, e74758 (2021).
87. J. P. Britt, F. Benaliouad, R. A. McDevitt, G. D. Stuber, R. A. Wise, A. Bonci, Synaptic and behavioral profile of multiple glutamatergic inputs to the nucleus accumbens. *Neuron* **76**, 790–803 (2012).
88. M. Shpokayte, O. McKissick, X. Guan, B. Yuan, B. Rahsepar, F. R. Fernandez, E. Ruesch, S. L. Grella, J. A. White, X. S. Liu, S. Ramirez, Hippocampal cells segregate positive and negative engrams. *Commun. Biol.* **5**, 1009 (2022).
89. R. Patel, R. N. Spreng, L. M. Shin, T. A. Girard, Neurocircuitry models of posttraumatic stress disorder and beyond: A meta-analysis of functional neuroimaging studies. *Neurosci. Biobehav. Rev.* **36**, 2130–2142 (2012).
90. C. G. Abdallah, K. M. Wrocklage, C. L. Averill, T. Akiki, B. Schweinsburg, A. Roy, B. Martini, S. M. Southwick, J. H. Krystal, J. C. Scott, Anterior hippocampal dysconnectivity in posttraumatic stress disorder: A dimensional and multimodal approach. *Transl. Psychiatry* **7**, e1045 (2017).
91. B. L. Malivoire, T. A. Girard, R. Patel, C. M. Monson, Functional connectivity of hippocampal subregions in PTSD: Relations with symptoms. *BMC Psychiatry* **18**, 129 (2018).
92. W. E. Skaggs, B. L. McNaughton, M. A. Wilson, C. A. Barnes, Theta phase precession in hippocampal neuronal populations and the compression of temporal sequences. *Hippocampus* **6**, 149–172 (1996).

Acknowledgments: We thank members of the Ciocchi laboratory and J. Jordan for discussions of the project. **Funding:** This work was supported by the European Research Council starting grant 716761 (S.C.) and Swiss National Science Foundation professorship grant 170654 (S.C.).
Author contributions: Conceptualization: R.N. and S.C. Methodology: R.N., K.K., and T.F. Investigation: R.N. Visualization: R.N. Funding acquisition: S.C. Project administration: R.N. Supervision: S.C. Writing (original draft): R.N. Writing (review and editing): R.N., S.C., T.F., and K.K.
Competing interests: The authors declare that they have no competing interests. **Data and materials availability:** All data needed to evaluate the conclusions in the paper are present in the paper and/or the Supplementary Materials and are available on Zenodo (https://doi.org/10.5281/zenodo.7754454).

Submitted 29 December 2022
Accepted 25 April 2023
Published 31 May 2023
10.1126/sciadv.adg4881

ScienceAdvances

Fear extinction relies on ventral hippocampal safety codes shaped by the amygdala

Robin Nguyen, Konstantinos Koukoutselos, Thomas Forro, and Stphane Ciocchi

Sci. Adv., **9** (22), eadg4881.
DOI: 10.1126/sciadv.adg4881

Science Advances (ISSN) is published by the American Association for the Advancement of Science. 1200 New York Avenue NW, Washington, DC 20005. The title *Science Advances* is a registered trademark of AAAS.